Electronic Supplementary Material (ESI) for Dalton Transactions.

Supplementary Information for:

Mapping the Influence of Ligand Electronics on the Spectroscopic and $^1O_2$ Sensitization Characteristics of Pd(II) Biladiene Complexes Bearing Phenyl-Alkynyl Groups at the 2- and 18-Postions

Maxwell I. Martin, Trong-Nhan Pham, Kaytlin N. Ward, Anthony T. Rice, Phoebe R. Hertler, Glenn P. A. Yap, Philip H. Gilmartin, and Joel Rosenthal*

Department of Chemistry and Biochemistry, University of Delaware, Newark, DE, 19716

Index		***Page***
	General Methods and Synthetic Protocols	**2–9**
Figures S1-S21	^{1}H, ^{19}F, ^{13}C{^{1}H} NMR Spectra for Synthesized Compounds	**10-20**
Figures S22-S25	Fully Labeled Crystal Structures for **Pd[DMBil2–R]** Derivatives	**21-22**
Figures S26-S30	Illustrations of Dihedral Angle Planes for Crystallized **Pd[DMBil2–R]** Derivatives	**23-25**
Table S1	Crystallographic Data for **Pd[DMBil2–R]** Derivatives	**26**
Figures S31-S32	Absorbance and Emission Spectra Recorded for **Pd[DMBil2–R]** Derivatives	**27-28**
Figure S33	Stacked DPVs Recorded for **Pd[DMBil1]** and **Pd[DMBil2–R]** Derivatives	**29**
Figure S34	Scatter Plots for *para*-Hammett Values and Redox Properties of **Pd[DMBil2–R]** Derivatives	**30**
Figure S35	Changes in absorbance Spectra recorded for **Pd[DMBil2–N(CH$_3$)$_2$]** upon addition of upto 500 equivalents of Trifluoroacetic Acid	**31**
	References	**32**

EXPERIMENTAL SECTION:

General Materials and Methods. Reactions requiring an inert atmosphere were carried out under positive pressure of N_2 using flasks fitted with Suba-Seal rubber septa and standard Schlenk techniques. Air and moisture sensitive reagents were transferred using standard syringe or cannula techniques. Reagents and solvents were purchased from Sigma Aldrich, Acros, Fisher, Strem, Oakwood, or Cambridge Isotopes Laboratories. **DMBil1**, **Pd[DMBil1]**, and **Pd[DMBilBr$_2$]** were synthesized according to published procedures.[1–6] Solvents used for synthesis were of reagent grade or better. Anhydrous solvents were dried by passage through activated alumina and stored over 4 Å molecular sieves prior to use. Column chromatography was performed with 40-63 μm silica gel from Silicycle.

Compound Characterization. ^{1}H NMR, ^{13}C{^{1}H} NMR, and ^{19}F NMR spectra were measured at 25 °C on a Bruker 400 MHz spectrometer with a cryogenic QNP probe. Proton spectra are refenced to the residual proton resonance of the deuterated solvent ($CDCl_3$ = δ 7.26) and carbon spectra are referenced to the carbon resonance of the solvent ($CDCl_3$ = δ 77.16).[7] Fluorine spectra are referenced to an external trifluoroacetic acid standard (TFA = δ –76.55 in CD_3CN).[8] All chemical shifts are reported using the standard δ notation in parts-per-million; positive chemical shifts are to higher frequency from given reference. Data are reported as follows: chemical shift, multiplicity (s = singlet, d = doublet, t = triplet, q = quartet, hept = heptet, m = multiplet), coupling constants, and number or protons. High-resolution mass spectrometry analyses were performed by the University of Delaware Mass Spectrometry Laboratory in the Department of Chemistry and Biochemistry.

Palladium 2,18-Diethynlbenzene-10,10-dimethyl-5,15-bis(pentafluorophenyl)-biladiene (Pd[DMBil2–H]): To a baked 100 mL Schlenk flask copper(I) iodide (4 mg, 0.021 mmol, 14 mol %) was added with a stir bar. The flask was placed under vacuum followed by addition of

of anhydrous triethylamine (3 mL) and phenylacetylene (164 ml, 1.5 mmol, 10 equiv) and stirring for 15 minutes at room temperature. Positive pressure of nitrogen gas was then applied and the septum was removed in order to add palladium 2,18-dibromo-10,10-dimethyl-5,15-dipentafluorophenylbiladiene (**Pd[DMBilBr$_2$]**) (138 mg, 0.15 mmol, 1.0 equiv) and tetrakis-palladium(0) triphenylphosphine (34 mg, 0.030 mmol, 20 mol %). The septum was then replaced and anhydrous tetrahydrofuran (40 mL) was cannula transferred into the flask, where upon the solution was stirred at 75°C for 16 hours. After the time elapsed, the solution was cooled to room temperature then exposed to air and diluted with 50 mL of ethyl acetate. The resulting solution was washed once with saturated ammonium chloride solution and once with brine, then dried over sodium sulfate and concentrated via rotary evaporation. The crude material was purified by column chromatography on silica using 10% CH_2Cl_2 in hexanes to yield 121 mg (0.13 mmol) target material as a maroon solid in 84% yield. ^{1}H NMR (400 MHz, $CDCl_3$, 25 °C) δ/ppm: 7.57 (s, 2H), 7.45 (d, 4H), 7.28 (m, 6H) 6.74 (d, *J* = 4.8 Hz, 2H), 6.69 (s, 2H), 6.61 (d, *J* = 4.8 Hz, 2H), 1.82 (s, 6H), 1.29 (s, 16H). ^{13}C{^{1}H} NMR (100 MHz, $CDCl_3$, 25 °C) δ/ppm: 168.4, 153.0, 136.0, 134.0, 132.3, 131.5, 129.8, 128.4, 128.1, 123.5, 118.1, 113.7, 91.9, 83.6, 42.1, 31.0. ^{19}F NMR (251 MHz, $CDCl_3$, 25 °C) δ/ppm: -137.8 (dt, *J* = 8.8, 5.2, 4F), -151.2 (dt, *J* = 8.8, 5.0 Hz, 2F), -160.0 (dt, *J* = 10.1, 3.8 Hz, 4F). HR-ESI-MS: $[M+H]^+$ *m/z*: calcd for $C_{49}H_{25}N_4F_{10}Pd$, 965.09758; found 965.09758.

*All other **Pd[DMBil2–R]** derivatives were synthesized using the same procedure, altering only the identity of the alkyne added and the chosen eluent for chromatography. Detailed methods of purification and characterization data for all other **Pd[DMBil2–R]** derivatives are provided below:*

Palladium 2,18-Bis(para-cyano-phenylethynyl)-10,10-dimethyl-5,15-dipentafluorophenylbiladiene (Pd[DMBil2–CN]): This compound was prepared on a 0.15 mmol scale from **Pd[DMBilBr$_2$]** and 4-cyanophenylacetylene following the method detailed for **Pd[DMBil2–H]**. The crude material was purified by column chromatography on silica using 10%

ethyl acetate in hexanes to yield 86 mg (0.085 mmol) of target material as a maroon solid in 57% yield. ^{1}H NMR (600 MHz, $CDCl_3$, 25 °C) δ/ppm: 7.57 (s, 2H), 7.56 (d, *J* = 8.4 Hz, 4H) 7.49 (d, *J* = 8.4 Hz, 4H), 6.79 (d, *J* = 4.6 Hz, 2H), 6.72 (s, 2H), 6.67 (d, *J* = 4.6 Hz, 2H), 1.83 (s, 6H). ^{13}C{^{1}H} NMR (151 MHz, $CDCl_3$, 25 °C) δ/ppm: 169.3, 152.2, 145.0 (d, *J* = 257.9 Hz), 136.5, 133.9, 133.1, 132.3, 132.2, 132.2, 132.1, 131.7, 129.8, 128.7, 128.6, 128.5, 118.9, 118.7, 112.3, 111.2, 90.3, 88.6, 42.4, 31.0. ^{19}F NMR (377 MHz, $CDCl_3$, 25 °C) δ/ppm: -138.4 (dd, *J* = 10.8, 3.8, 4F), -151.2 (t, *J* = 13.8, 2F), -160.3 (dt, *J* = 13.8, 3.8, 4F). HR-ESI-MS: $[M+H]^+$ *m/z*: calcd for $C_{51}H_{22}N_6F_{10}Pd$, 1015.08593; found 1015.08828.

Palladium 2,18-Bis(para-trifluoromethyl-phenylethynyl)-10,10-dimethyl-5,15-dipentafluorophenylbiladiene (Pd[DMBil2–CF_3]): This compound was prepared on a 0.15 mmol scale from **Pd[DMBilBr_2]** and 4-trifluoromethylphenylacetylene following the method detailed for **Pd[DMBil2–H]**. The crude material was purified by column chromatography on silica using 10% ethyl acetate in hexanes to yield 127 mg (0.12 mmol) of target material as a purple solid in 77% yield. ^{1}H NMR (400 MHz, $CDCl_3$, 25 °C) δ/ppm: 7.57 (s, 2H), 7.54 (s, 8H), 6.78 (d, *J* = 4.6 Hz, 2H), 6.72 (s, 2H), 6.65 (d, *J* = 4.6 Hz, 2H), 1.83 (s, 6H). ^{13}C{^{1}H} NMR (100 MHz, $CDCl_3$, 25 °C) δ/ppm: 168.9, 152.4, 136.2, 133.8, 132.7, 131.4, 129.7, 129.6, 128.6, 127.3, 125.3, 125.2, 125.1, 122.3, 118.5, 112.6, 90.4, 86.2, 42.2, 30.8. ^{19}F NMR (251 MHz, $CDCl_3$, 25 °C) δ/ppm: -62.2 (s, 6F), -137.9 (dd, *J* = 9.4, 3.8, 4F), -150.9 (t, *J* = 12.6, 2F), -159.8 (dt, *J* = 12.6, 3.8, 4F). HR-ESI-MS: $[M+H]^+$ *m/z*: calcd for $C_{51}H_{23}N_4F_{16}Pd$, 1101.07021; found 1101.07022.

Palladium 2,18-Bis(para-methyl-ester-phenylethynyl)-10,10-dimethyl-5,15-dipentafluorophenylbiladiene (Pd[DMBil2–CO_2CH_3]): This compound was prepared on a 0.15 mmol scale from **Pd[DMBilBr_2]** and 4-(methoxycarbonyl)phenylacetylene following the method detailed for **Pd[DMBil2–H]**. The crude material was purified by column chromatography on silica using 10% ethyl acetate in hexanes to yield 118 mg (0.11 mmol) of target material as a maroon solid in 73% yield. ^{1}H NMR (400 MHz, $CDCl_3$, 25 °C) δ/ppm: 7.96 (d, *J* = 8 Hz, 4H), 7.57 (s, 2H),

7.49 (d, *J* = 8 Hz, 4H), 6.78 (d, *J* = 4.6 Hz, 2H), 6.72 (s, 2H), 6.64 (d, *J* = 4.6 Hz, 2H), 3.90 (s, 6H), 1.83 (s, 6H). $^{13}C\{^{1}H\}$ NMR (100 MHz, $CDCl_3$, 25 °C) δ/ppm: 168.9, 168.7, 152.6, 136.3, 133.9, 132.7, 131.2, 129.9, 129.6, 129.2, 128.7, 128.3, 118.5, 112.9, 91.3, 87.0, 52.4, 42.3, 31.0. ^{19}F NMR (251 MHz, $CDCl_3$, 25 °C) δ/ppm: -137.8 (dd, *J* = 9.4, 3.8, 4F), -150.9 (t, *J* = 13.8, 2F), -159.9 (dt, *J* = 13.8, 3.8, 4F). HR-ESI-MS: $[M+H]^+$ *m/z*: calcd for $C_{53}H_{41}N_4F_{10}O_4Pd$, 1025.11657; found 1025.11705.

Palladium 2,18-Bis(para-tert-butyl-phenylethynyl)-10,10-dimethyl-5,15-dipentafluorophenylbiladiene (Pd[DMBil2–*t*-Bu]): This compound was prepared on a 0.15 mmol scale from **Pd[DMBilBr$_2$]** and 4-*tert*-butylphenylacetylene following the method detailed for **Pd[DMBil2–H]**. The crude material was purified by column chromatography on silica using 10% CH_2Cl_2 in hexanes to yield 130 mg (0.12 mmol) of target material as a maroon solid in 81% yield. ^{1}H NMR (400 MHz, $CDCl_3$, 25 °C) δ/ppm: 7.57 (s, 2H), 7.26 (d, *J* = 9.6 Hz, 4H), 7.31 (*J* = 9.6 Hz, 6H) 6.75 (d, *J* = 4.6 Hz, 2H), 6.71 (s, 2H), 6.62 (d, *J* = 4.6Hz, 2H), 1.83 (s, 6H). $^{13}C\{^{1}H\}$ NMR (100 MHz, $CDCl_3$, 25 °C) δ/ppm: 168.2, 153.2, 151.3, 145.0 (d, *J* = 246.2 Hz), 141. 9 (d, *J* = 248.4 Hz), 137.5 (d, *J* = 254.7 Hz), 135.9, 134.0, 132.1, 131.2, 129.7, 128.4, 125.4, 120.5, 117.9, 114.1, 111.9 (t, *J* = 19.0 Hz), 92.1, 82.9, 77.4, 42.1, 36.7, 34.9, 31.6, 31.3, 31.0. ^{19}F NMR (251 MHz, $CDCl_3$, 25 °C) δ/ppm: -138.3 (dd, *J* = 11.3, 3.8, 4F), -151.8 (t, *J* = 13.8, 2F), -160.6 (dt, *J* = 13.8, 3.8, 4F). HR-LIFDI-MS: $[M+H]^+$ *m/z*: calcd for $C_{57}H_{40}N_4F_{10}Pd$, 1076.2128; found 1076.1862.

Palladium 2,18-Bis(para-methoxy-phenylethynyl)-10,10-dimethyl-5,15-dipentafluorophenylbiladiene (Pd[DMBil2–OCH$_3$]): This compound was prepared on a 0.15 mmol scale from **Pd[DMBilBr$_2$]** and 4-methoxyphenylacetylene following the method detailed for **Pd[DMBil2–H]**. The crude material was purified by column chromatography on silica using 15% ethyl acetate in hexanes to yield 132 mg (0.13 mmol) of target material as a purple solid in 86% yield. ^{1}H NMR (400 MHz, $CDCl_3$, 25 °C) δ/ppm: 7.57 (s, 2H), 7.45 (m, 4H), 7.28 (m, 4H), 6.78 (d, *J* = 4.6 Hz, 2H), 6.74 (s, 2H), 6.61 (d, *J* = 4.6 Hz, 2H), 3.79 (s, 6H), 1.82 (s, 6H). $^{13}C\{^{1}H\}$ NMR

(100 MHz, $CDCl_3$, 25 °C) δ/ppm: 168.2, 152.8, 145.0 (d, *J* = 251.0 Hz), 141.9 (d, *J* = 256.4 Hz), 137.5 (d, *J* = 255.6 Hz) 136.2, 134.1, 132.5, 131.8, 131.5, 129.9, 129.4, 128.4, 128.0, 123.6, 117.8, 113.4, 111.9 (t, *J* = 20.9 Hz) , 91.7, 83.9, 61.9, 42.1, 31.0. ^{19}F NMR (251 MHz, $CDCl_3$, 25 °C) δ/ppm: -138.3 (dd, *J* = 10.0, 3.8, 4F), -151.8 (t, *J* = 13.8, 2F), -160.6 (dt, *J* = 13.8, 3.8, 4F). HR-ESI-MS: $[M+H]^+$ *m/z*: calcd for $C_{51}H_{29}N_4F_{10}O_2Pd$, 1081.10640; found 1081.11003.

Palladium 2,18-Bis(para{N,N-dimethyl-amino}-phenylethynyl)-10,10-dimethyl-5,15-dipentafluorophenylbiladiene (Pd[DMBil2–N(CH_3)$_2$]): This compound was prepared on a 0.15 mmol scale from **Pd[DMBilBr$_2$]** and 4-dimethylaminophenylacetylene following the method detailed for **Pd[DMBil2–H]**. The crude material was purified by column chromatography on silica using 10% ethyl acetate in hexanes to yield 102 mg (0.097 mmol) of target material as a purple solid in 67% yield. ^1H NMR (400 MHz, $CDCl_3$, 25 °C) δ/ppm: 7.56 (s, 2H), 7.34 (d, *J* = 9 Hz, 4H), 6.70 (d, *J* = 4.6 Hz, 2H), 6.65 (s, 2H), 6.61 (d, *J* = 9 Hz, 4H), 6.59 (d, *J* = 4.6 Hz, 2H), 2.96 (s, 12H), 1.82 (s, 6H). $^{13}C\{^1H\}$ NMR (100 MHz, $CDCl_3$, 25 °C) δ/ppm: 167.6, 153.6, 150.0, 1465. 0 (d, *J* = 249.8 Hz) , 137.5 (d, *J* = 256.4 Hz), 135.7, 134.1, 132.8, 132.6, 131.6, 129.3, 128.0, 117.4, 114.9, 111.9, 110.3, 93.2, 81.4, 41.9, 40.4, 31.0. ^{19}F NMR (251 MHz, $CDCl_3$, 25 °C) δ/ppm: -137.8 (dd, *J* = 11.3, 3.8, 4F), -151.6 (t, *J* = 13.8, 2F), -160.2 (dt, *J* = 13.8, 3.8, 4F). HR-ESI-MS: $[M+H]^+$ *m/z*: calcd for $C_{53}H_{35}N_6F_{10}Pd$, 1051.17984; found 1051.18292.

Electrochemical Experiments. All cyclic voltammetry (CV) and differential pulse voltammetry (DPV) experiments were performed using a CHI-620D potentiostat and a standard three-electrode setup consisting of a glassy-carbon disk working electrode (3.0 mm diameter), a platinum mesh counter electrode, and a leakless Ag/AgCl reference electrode (in 3.4 M KCl solution) purchased from eDAQ. Measurements were collected in anhydrous acetonitrile solutions containing 0.1 M $TBAPF_6$ as supporting electrolyte. Each of the **Pd[DMBil1]** and **Pd[DMBil2–R]** derivatives were analyzed at a concentration of 1.0 mM. Solutions were sparged with argon for 20 minutes before data collection was performed while maintining positive pressure of argon over

the electrochemical cell. Freshly sublimed ferrocene was added to the electrolyte solutions at the end of the CV and DPV data collections as an internal standard. All reported potentials are referenced relative to Fc/Fc^+. Reported CV and DPV experiments were carried out at a scan rate of ν =100 mV s^{-1}.

X-ray Structural Analysis. Crystals of **Pd[DMBil2–H]**, **Pd[DMBil2–OCH_3]**, **Pd[DMBil2–CF_3]**and **Pd[DMBil2–CN]** were obtained via slow evaporation of saturated solutions of the respective complexes in 50:50 mixtures of methanol and CH_2Cl_2. Crystals were mounted on plastic mesh using viscous oil and cooled to the data collection temperature. Data were collected on either a Bruker-AXS Apex III DUO CCD diffractometer with graphite monochromated Mo-Kα radiation (λ = 0.71073 Å) or on a D8 Venture with microfocused Cu-K Kα radiation (λ = 1.54178 Å). Unit cell parameters were obtained from 36 data frames, 0.5° ω, from different sections of the Ewald sphere or a hemisphere fast scan, 1° ω/s .[9] The systematic absences from the diffraction data were consistent for *Cc* and *C*2/*c* for **Pd[DMBil2–CN]** and **Pd[DMBil2–OCH_3]**, and, uniquely, for $P2_1/n$ for **Pd[DMBil2–CF_3]**. No symmetry higher than triclinic was observed for **Pd[DMBil2–H]**. Solution in the centrosymmetric space group options for **Pd[DMBil2–OCH_3]** and **Pd[DMBil2–H]**, *C*2/*c* and *P*-1, respectively, yielded chemically reasonable and computationally stable results of refinement. Only the noncentrosymmetric option *Cc* yielded chemically reasonable results for **Pd[DMBil2–CN]**. The data were treated with multi-scan absorption corrections.[9] The structures were solved using intrinsic phasing methods[10] and refined with full-matrix, least-squares procedures on F^2.[11] Three half molecules of the compound were located in the asymmetric unit of **Pd[DMBil2–CN].** Two compound molecules and a toluene molecule of solvation was found in the asymmetric unit of **Pd[DMBil2–CF_3].** Non-hydrogen atoms were refined with anisotropic displacement parameters. H-atoms were constrained in idealized positions with isotropic parameters based on their attached atoms (1.2 -1.5 U_{eq}). The penultimate difference maps were treated with Squeeze to model disordered solvent molecules as diffused contributions.[12] Atomic

scattering factors are contained in the SHELXTL program library.[11] The structures have been deposited at the Cambridge Structural Database under deposition numbers CCDC 2096341–2096344.

UV–Visible Absorption Experiments. All UV–visible absorbance spectra were collected at room temperature on a StellarNet CCD array UV–visible spectrometer using quartz cuvettes (6Q) was a 1.0 cm path length from Starna Cells, Inc. Absorption spectra of all species were collected in methanol at concentrations of 3.0, 6.0, 9.0, 12.0, and 15.0 μM.

Emission Experiments. Emission spectra were recorded on an automated Photon Technology International (PTI) QuantaMaser 40 fluorometer equipped with a 75 W xenon arc lamp, an LPS-220B lamp power supply, and a Hamamatsu R2658 photomultiplier tube. All samples were prepared in screw cap quartz cuvettes of 1.0 cm path length from Starna Cells, Inc. The samples were excited at λ_{ex} = 500 nm, and emission was monitored from λ_{em} = 515 to 1000 nm using a step size of 1 nm and an integration time of 0.25 s.

Emission quantum yields were calculated using a solution of $[Ru(bpy)_3][PF_6]_2$ in nitrogen saturated acetonitrile as reference and the expression below:

$$\Phi_s = \Phi_{ref}\left(\frac{I_s}{I_{ref}}\right)\left(\frac{A_{ref}}{A_S}\right)\left(\frac{\eta_S}{\eta_{ref}}\right)^2$$

where Φ_S and Φ_{ref} are the emission quantum yields of the sample and the reference (Φ_{ref} = 0.094 for $[Ru(bpy)_3][PF_6]_2$ in acetonitrile)[13,14], respectively, I_s and I_{ref} are the integrated emission intensities of the samples and reference, A_s and A_{ref} are the measured absorbances of the sample and reference at the excitation wavelength, and η_s and η_{ref} are the refractive indices of the solvents used for the sample and reference.

Singlet Oxygen Sensitization Quantum Yield Determination. $^1O_2$ production was quantified by monitoring the fluorescence quenching of 1,3-diphenylisobenzofuran (DPBF), a

previously studied $^1O_2$ trapping agent. Measurements were carried out on an automated Photon Technology International (PTI) QuantaMaster 40 fluorometer equipped with a 75-W Xenon arc lamp, an LPS-220B lamp power supply and a Hammamatsu R2658 photomultiplier tube using quartz cuvettes (6Q) of 1.0 cm path length. Each cuvette contained 3.0 mL of methanol solution that was 10.0 μM in **Pd[DMBil2–R]** or methylene blue (used as a reference, Φ_D = 0.51)[15] and 1.0 μM in DPBF. An additional cuvette containing only methanol and 1.0 μM DPBF was used as a control. Consumption of DPBF was monitored by observing the change in its integrated emission intensity following irradiation with light from an Intralux 9000 light source (Volpi) fitted with a 10 nm (fwhm) bandpass filter centered at 600 nm (Thor Labs, FB600-10). During the studies, each cuvette was irradiated for 5 second intervals for a total of 30 seconds. DPBF emission spectra were obtained by exciting at λ_{ex} = 405 nm and scanning from λ_{em} = 400 – 600 nm using a step size of 1 nm and an integration time of 0.25 nm seconds.

Calibration curves of the integrated emission intensity versus the concentration of unreacted DPBF remaining in solution were generated to correct for the absorption of the photosensitizers and standard between 400 – 600 nm. Emission spectra were collected from 10 μM solutions of **Pd[DMBil2–R]** or methylene blue containing DPBF concentrations of 0.3, 0.6, 0.9, 1.2, and 1.5 μM. Linear regression lines fit to the calibration data from each solution enabled the integrated emission intensity values obtained from the $^1O_2$ sensitization experiments to be converted into the corresponding concentrations of unreacted DPBF. A final plot of the concentration of unreacted DPBF versus irradiation time formed a straight line of slope m, which allowed for calculation of the $^1O_2$ quantum yields via the following expression:

$$\Phi_s = \Phi_{ref} \frac{m_s}{m_{ref}} \frac{\varepsilon_{ref}}{\varepsilon_s}$$

Where Φ_s and Φ_{ref} are the $^1O_2$ sensitization quantum yields for the sample and methylene blue reference (51% in methanol),[15] respectively, m_s and m_{ref} are the slopes of the concentration of

unreacted DPBF vs. irradiation time plots for the sample and reference, and ε_s and ε_{ref} are the extinction coefficients at the wavelength of irradiation (600 nm) for the sample and reference. All reported $^1O_2$ quantum yields were obtained from an average of three trials.

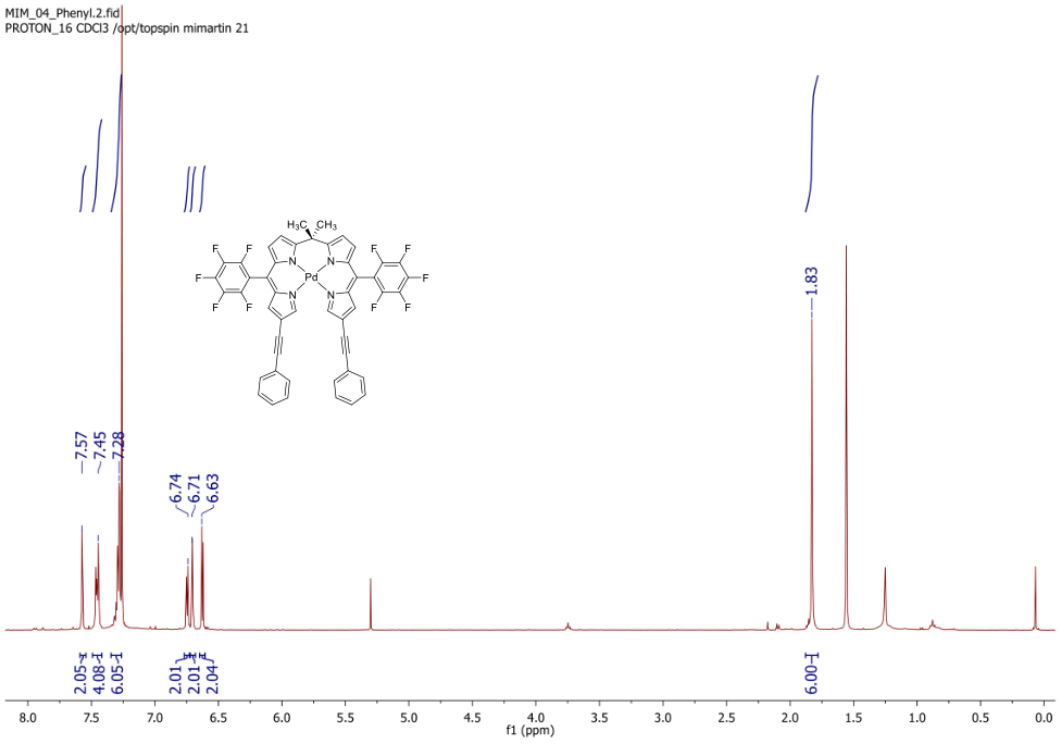

Figure S1. ^{1}H NMR of **Pd[DMBil2–H]**

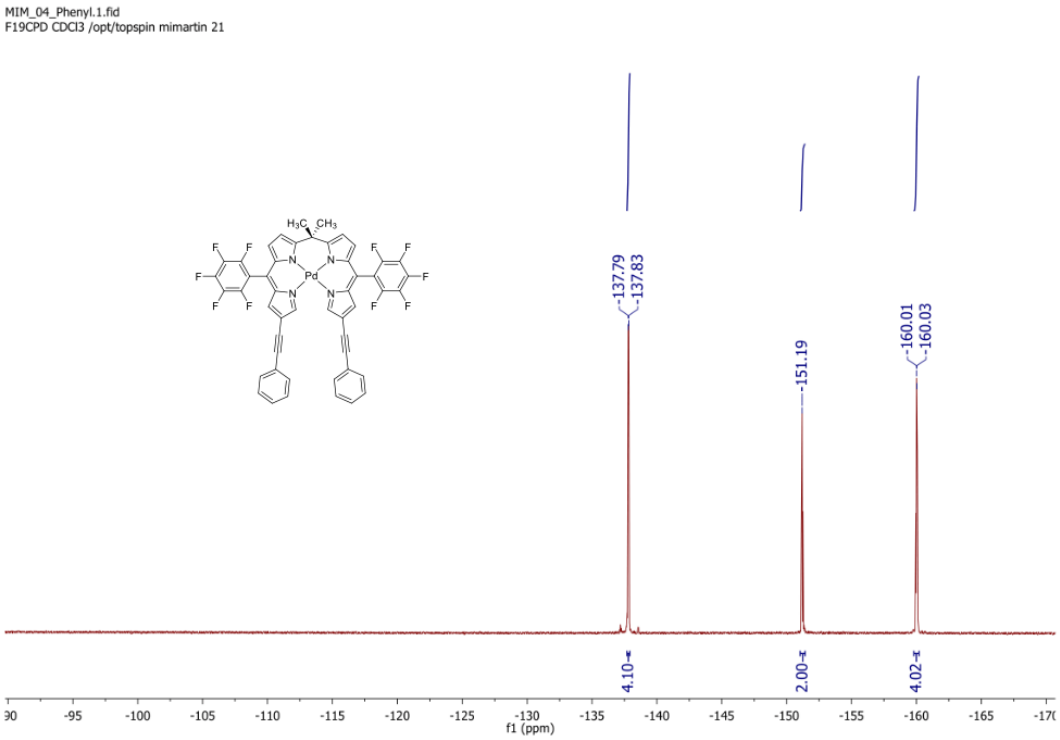

Figure S2. ^{19}F NMR of **Pd[DMBil2–H]**

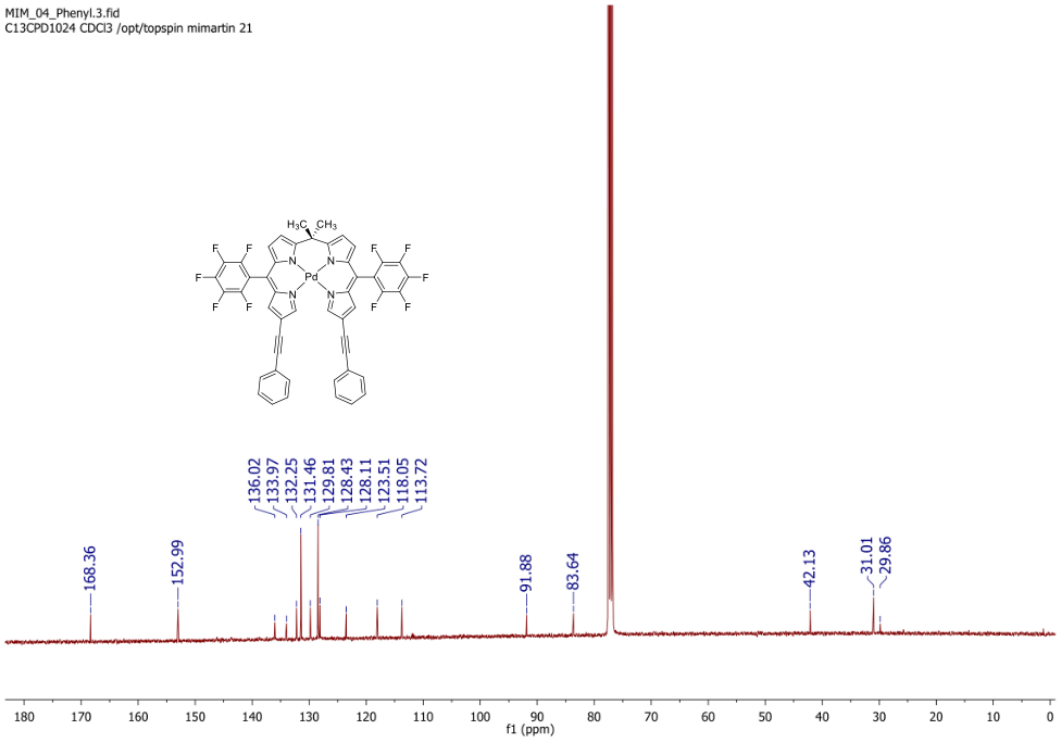

Figure S3. ^{13}C{^{1}H} NMR of **Pd[DMBil2–H]**

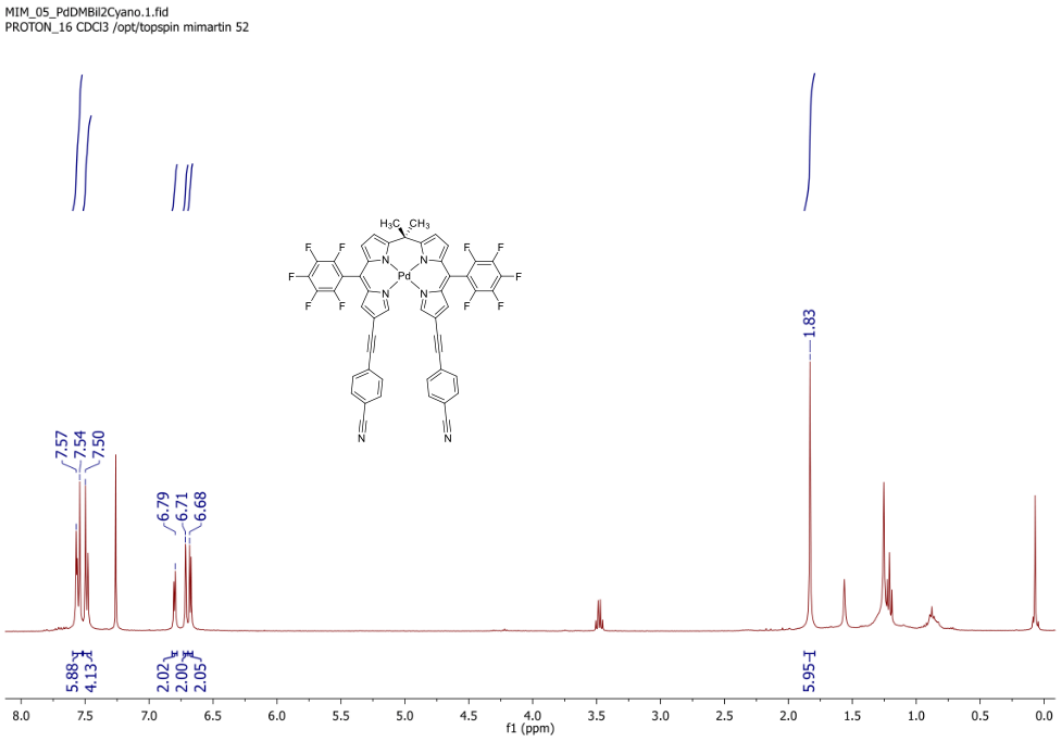

Figure S4. ^{1}H NMR of **Pd[DMBil2–CN]**

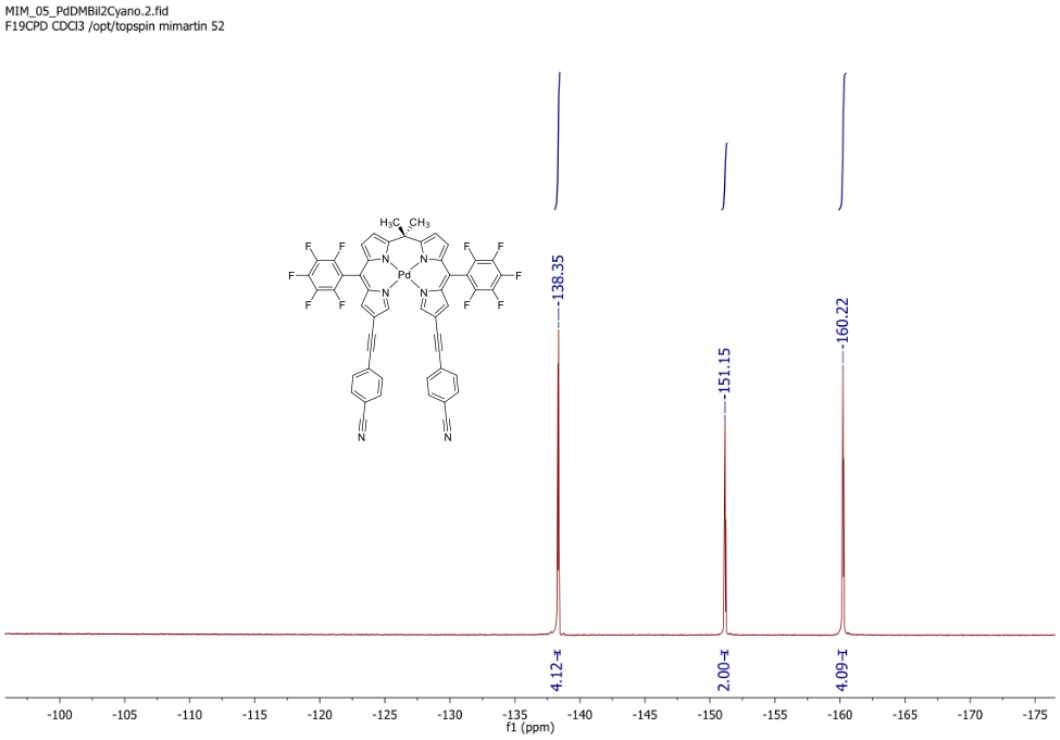

Figure S5. ^{19}F NMR of **Pd[DMBil2–CN]**

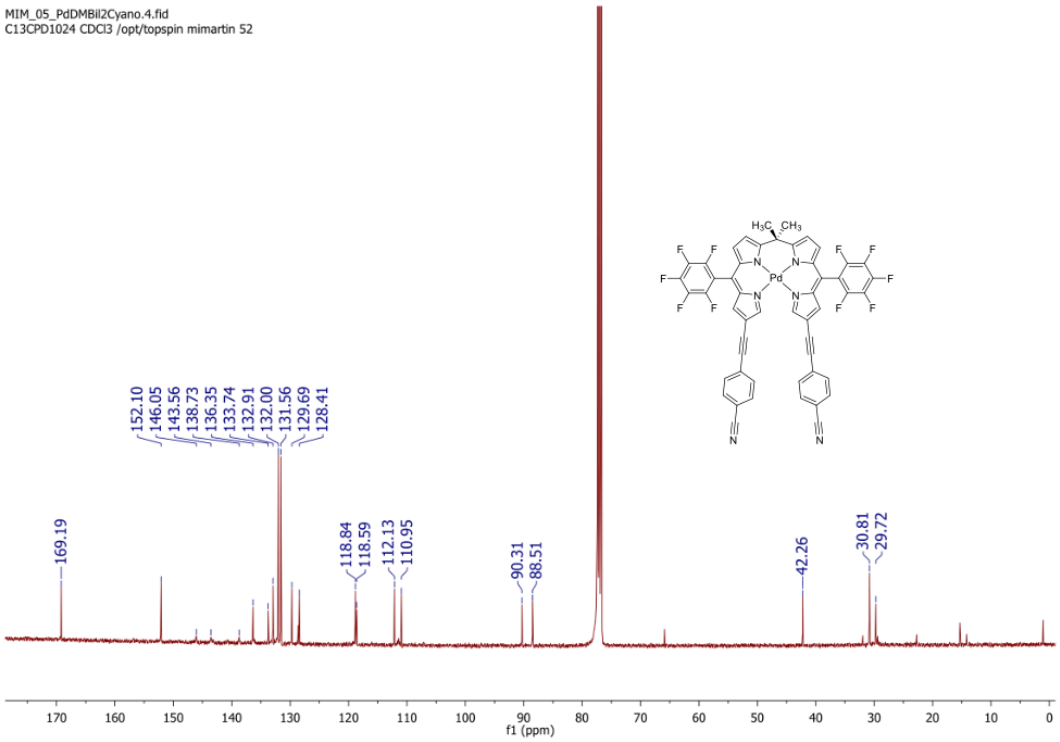

Figure S6. $^{13}C\{^{1}H\}$ NMR of **Pd[DMBil2–CN]**

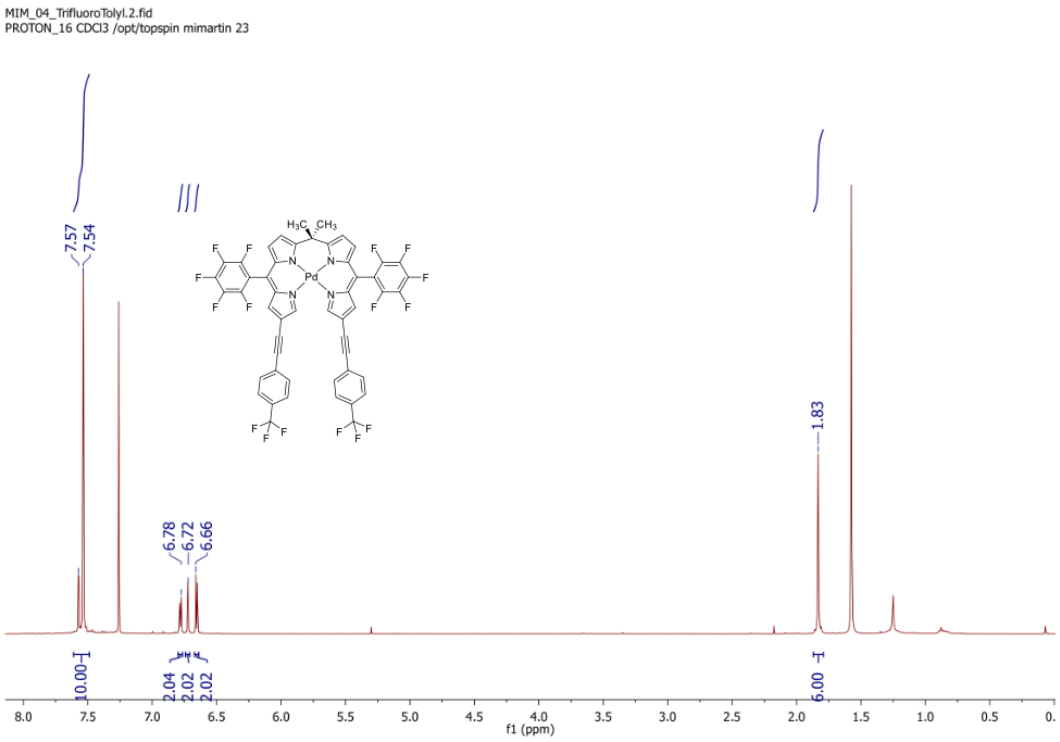

Figure S7. ^{1}H NMR of **Pd[DMBil2–CF_3]**

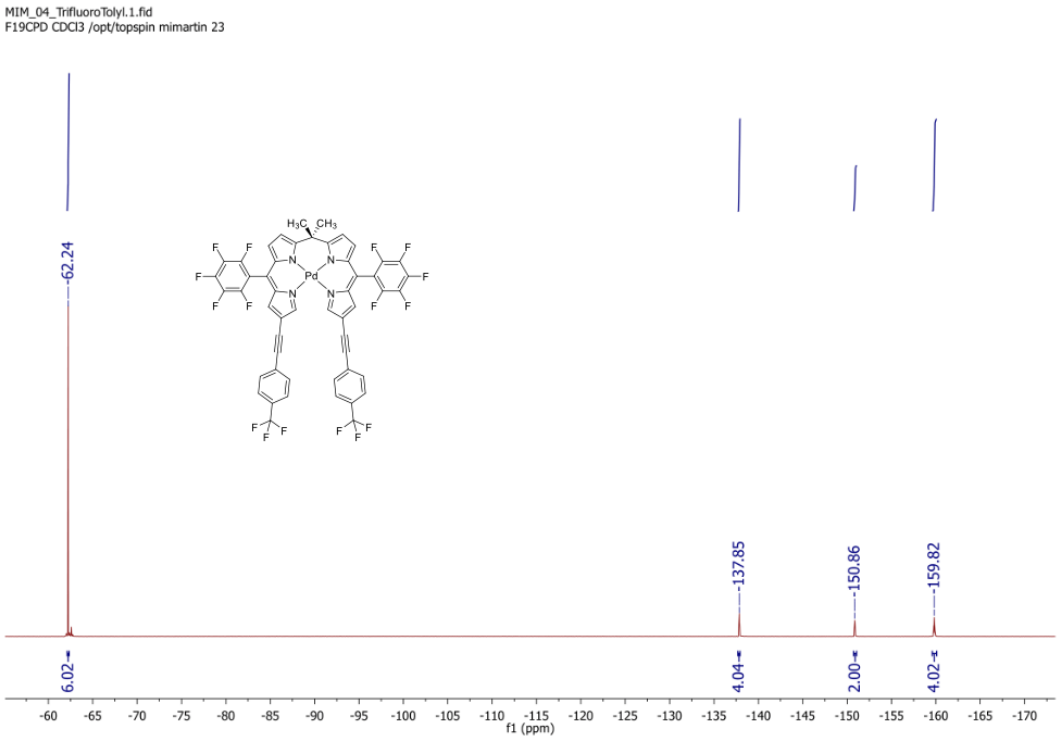

Figure S8. ^{19}F NMR of **Pd[DMBil2–CF_3]**

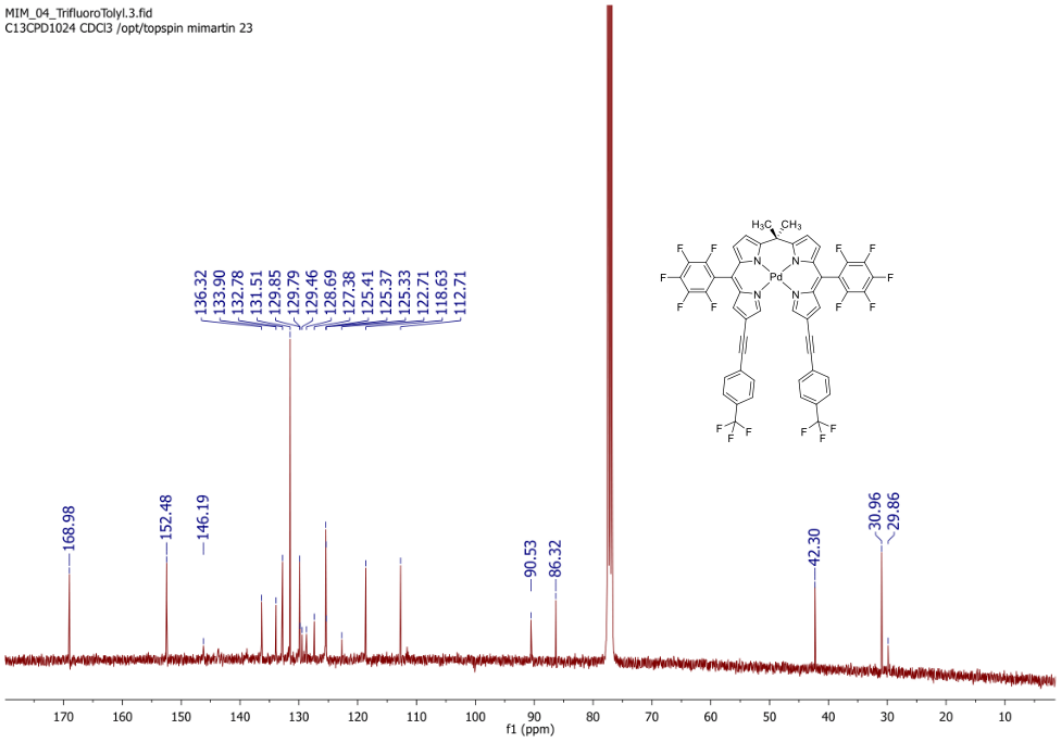

Figure S9. $^{13}C\{^1H\}$ NMR of **Pd[DMBil2–CF_3]**

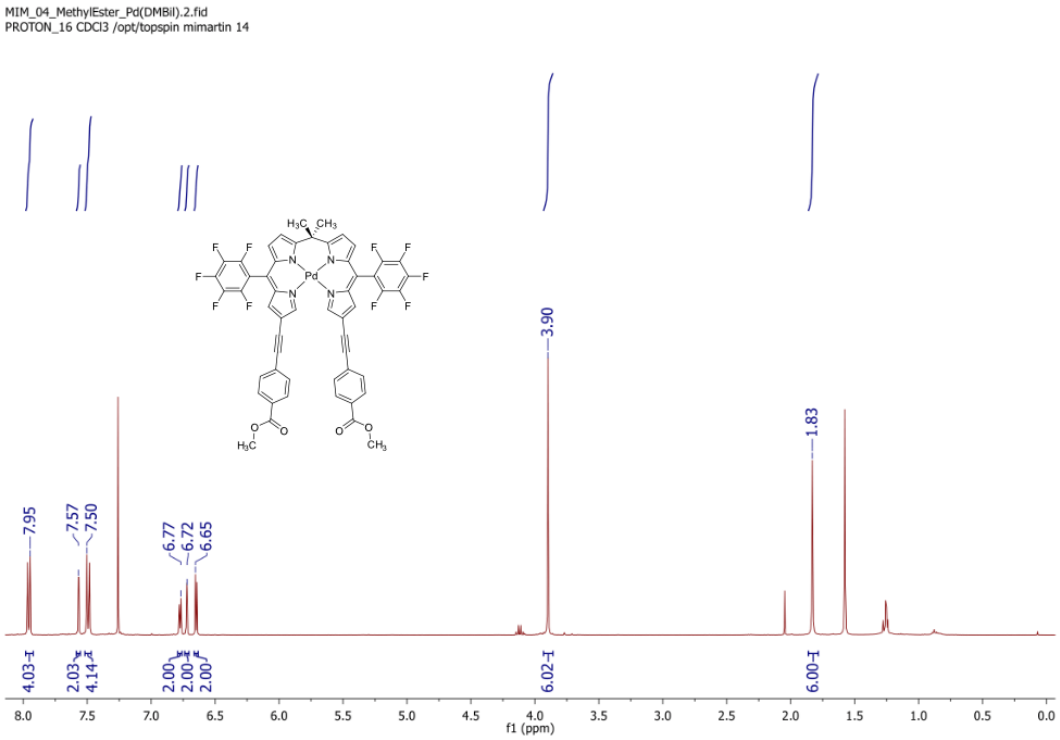

Figure S10. ^{1}H NMR of **Pd[DMBil2–CO_2CH_3]**

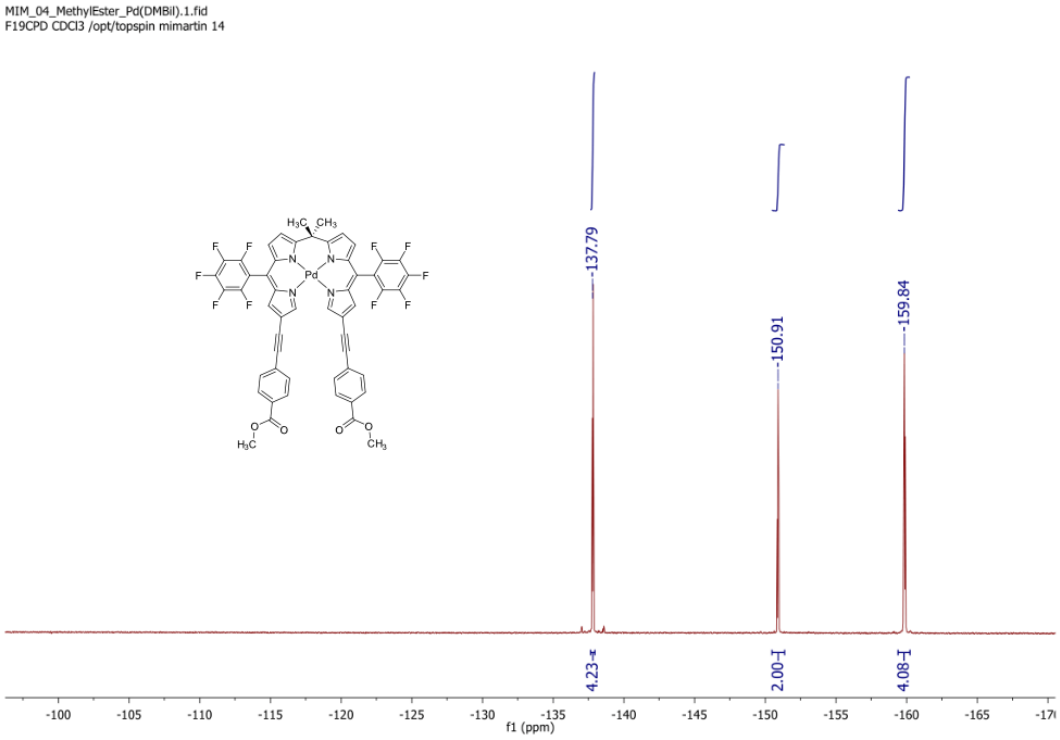

Figure S11. ^{19}F NMR of **Pd[DMBil2–CO_2CH_3]**

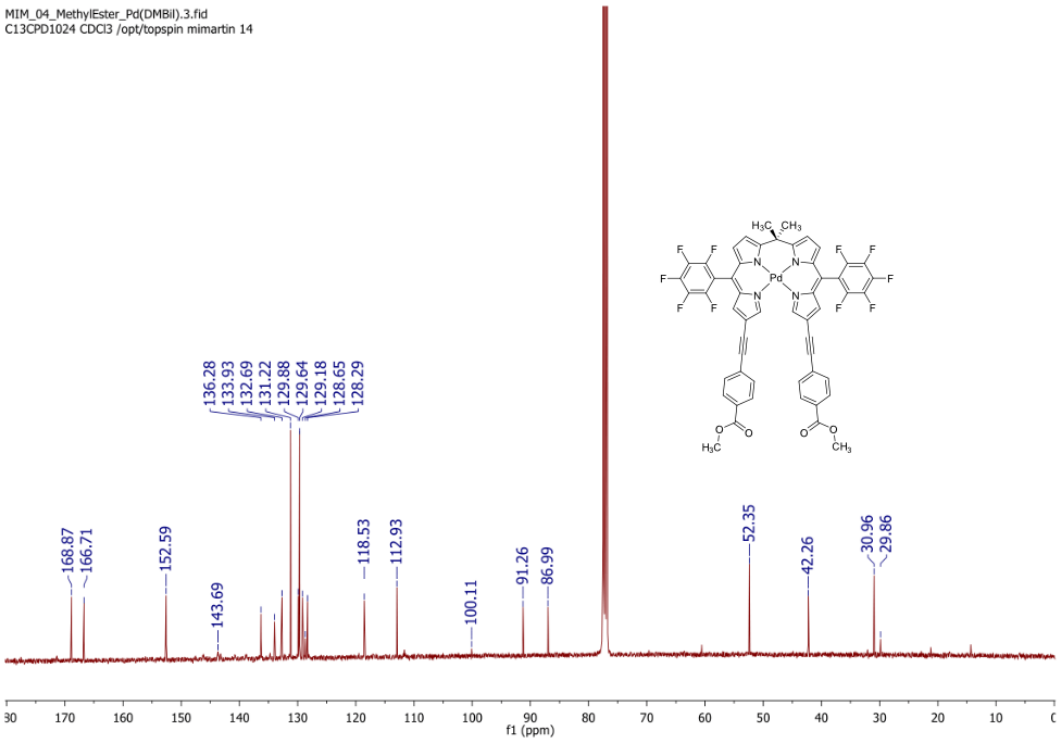

Figure S12. $^{13}C\{^{1}H\}$ NMR of **Pd[DMBil2–CO_2CH_3]**

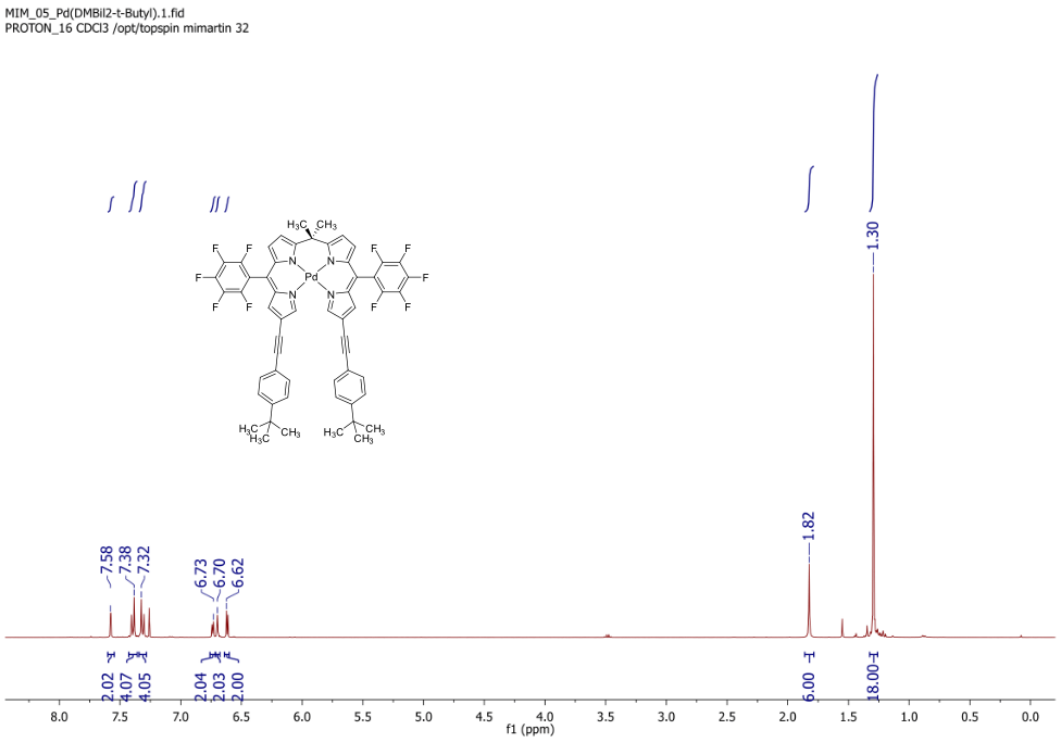

Figure S13. ^{1}H NMR of **Pd[DMBil2–$C(CH_3)_3$]**

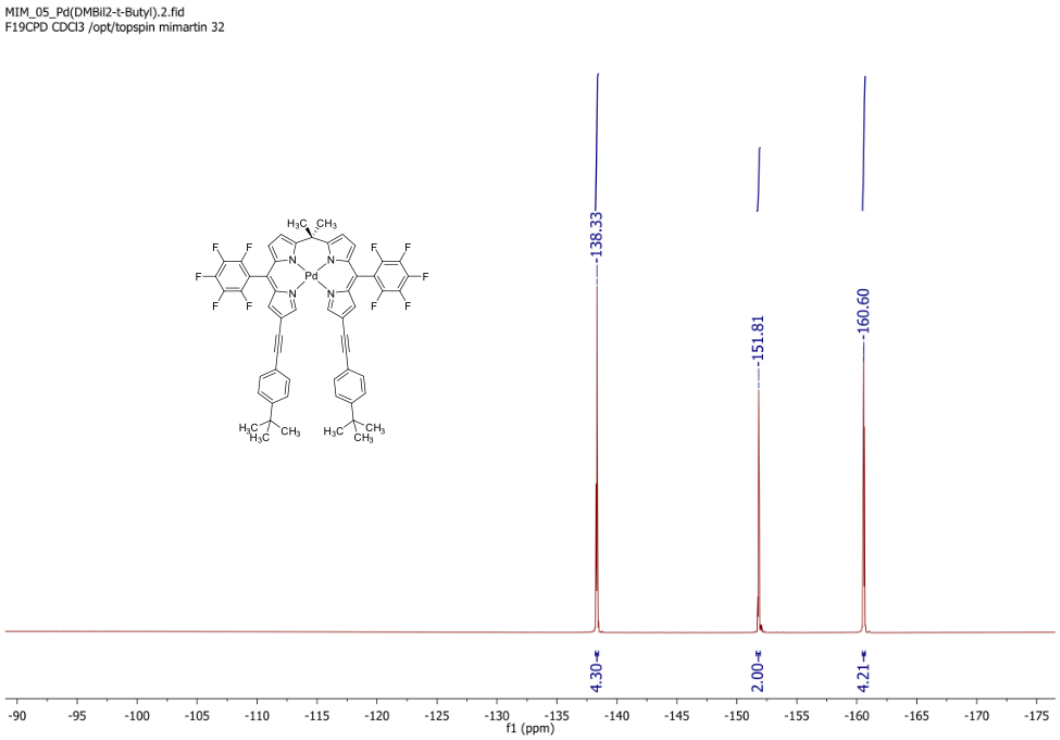

Figure S14. ^{19}F NMR of **Pd[DMBil2–C(CH$_3$)$_3$]**

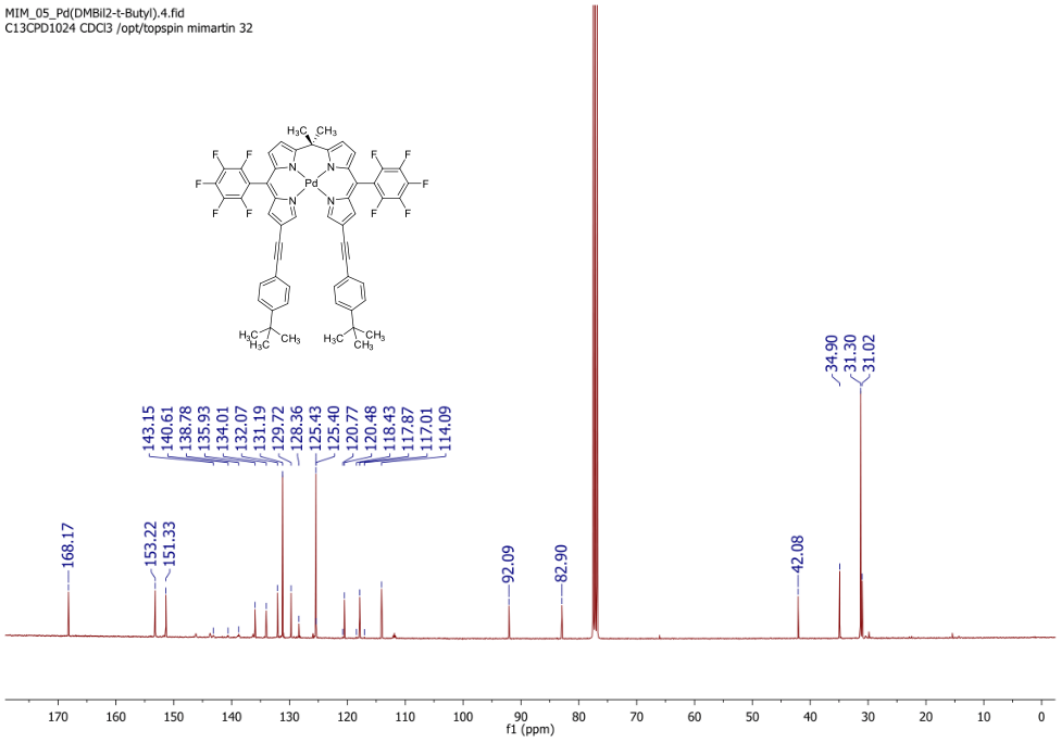

Figure S15. ^{13}C{^{1}H} NMR of **Pd[DMBil2–C(CH$_3$)$_3$]**

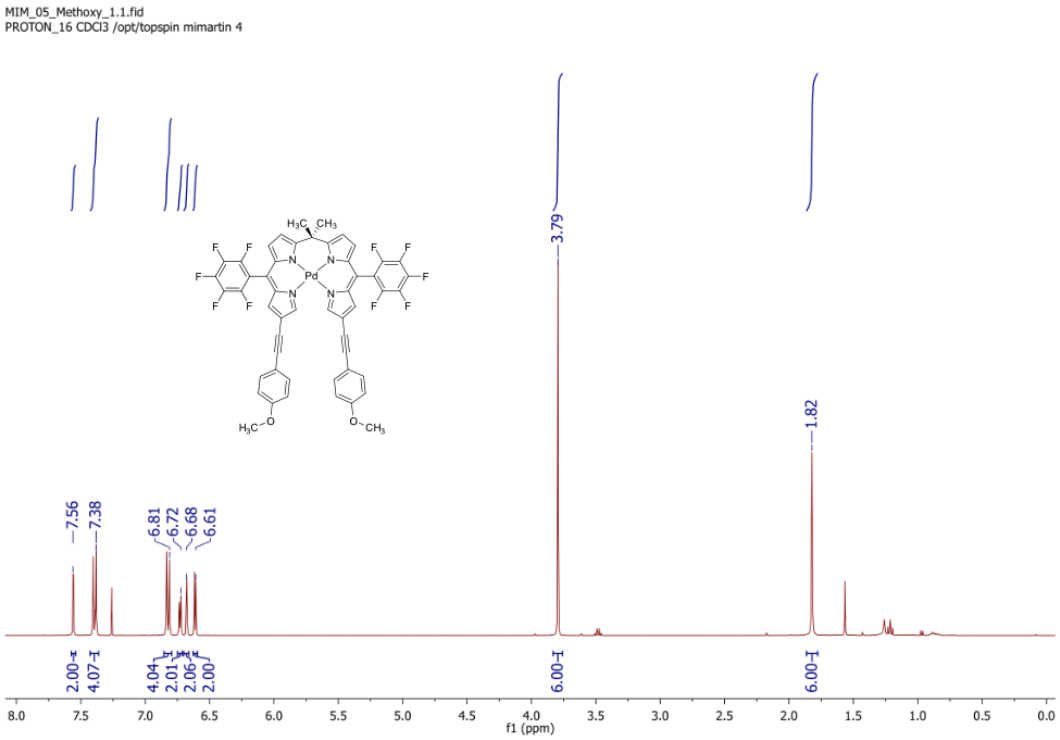

Figure S16. ^{1}H NMR of **Pd[DMBil2–OCH$_3$]**

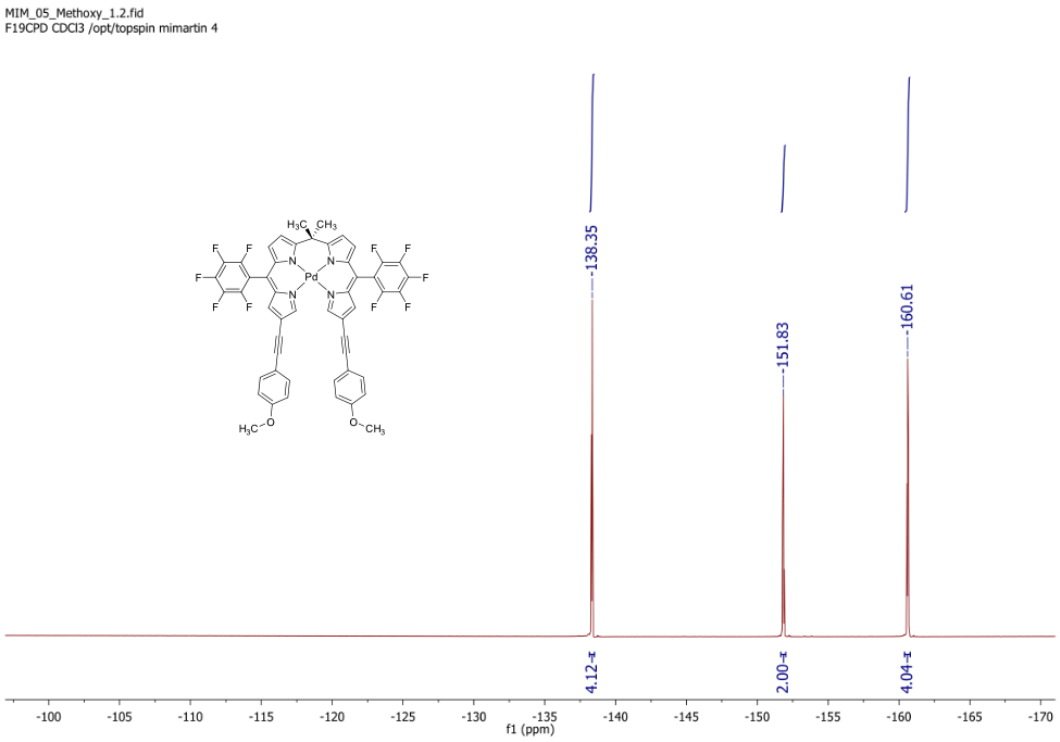

Figure S17. ^{19}F NMR of **Pd[DMBil2–OCH$_3$]**

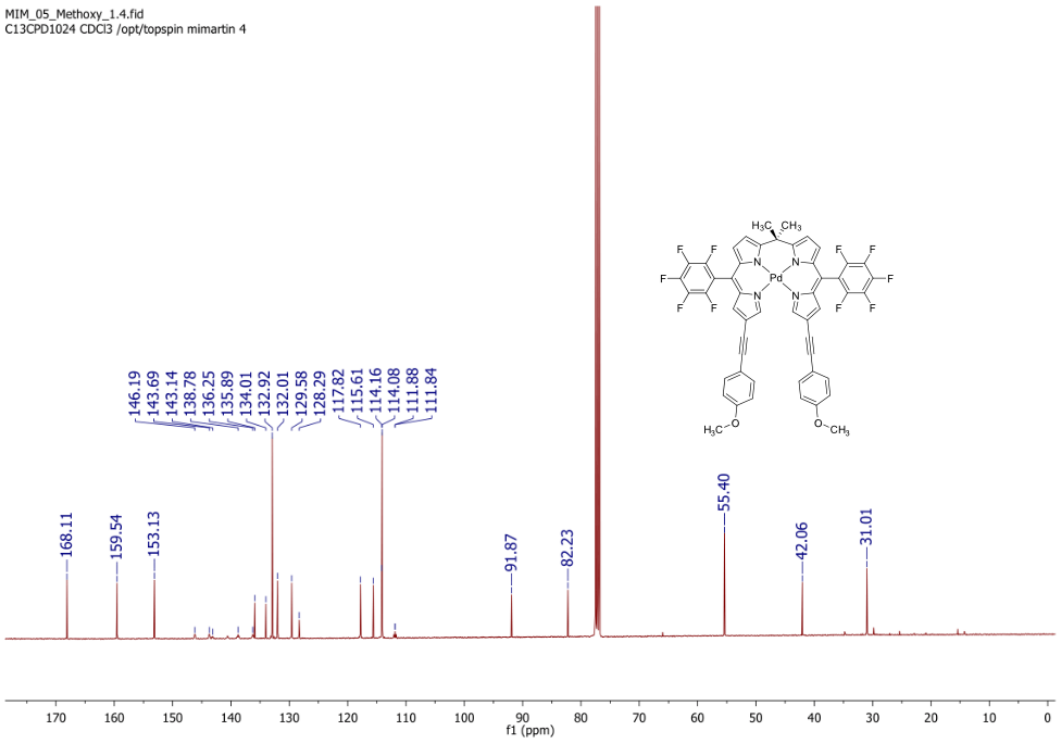

Figure S18. $^{13}C\{^{1}H\}$ NMR of **Pd[DMBil2–OCH$_3$]**

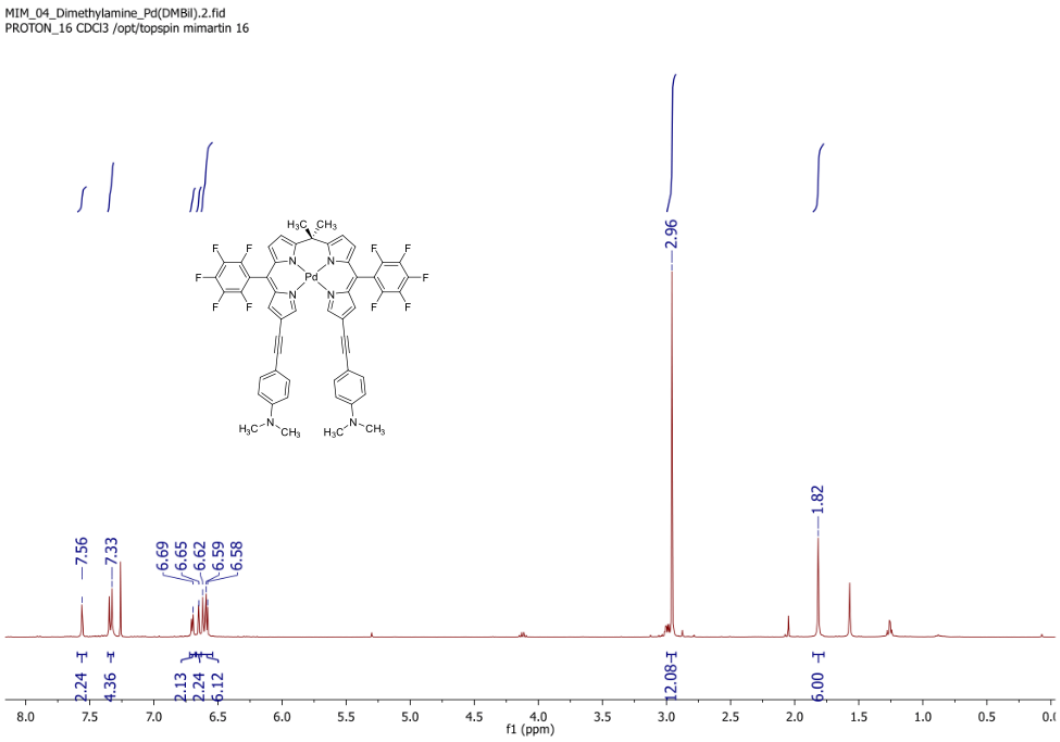

Figure S19. ^{1}H NMR of **Pd[DMBil2–N(CH$_3$)$_2$]**

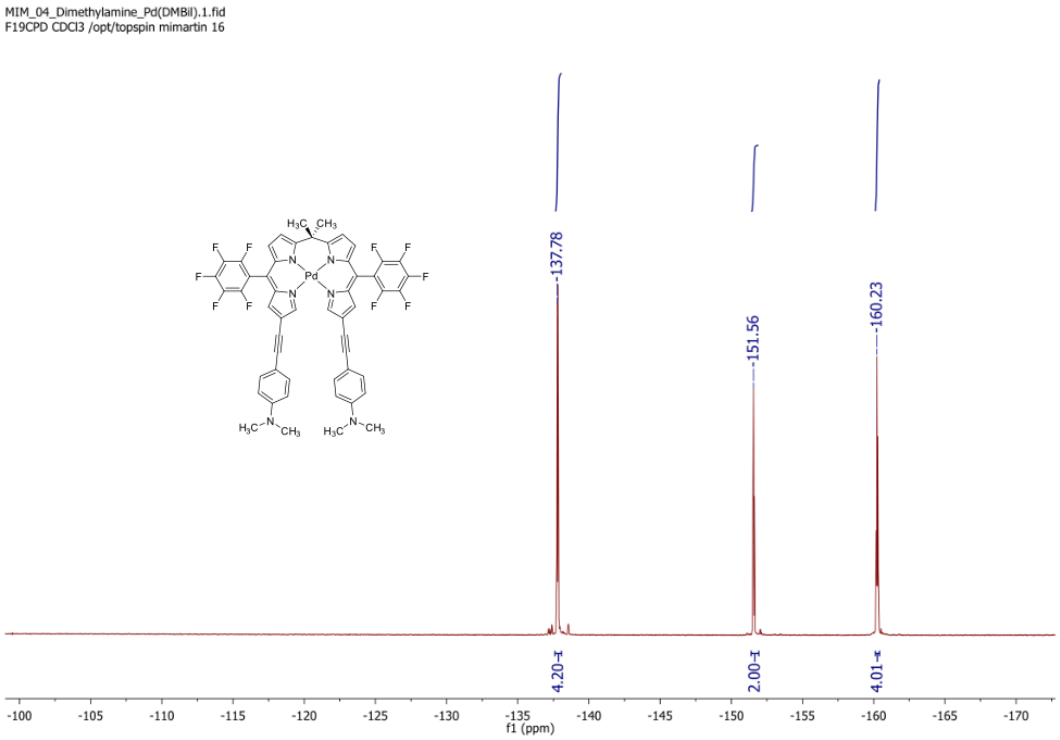

Figure S20. ^{19}F NMR of **Pd[DMBil2–N(CH$_3$)$_2$]**

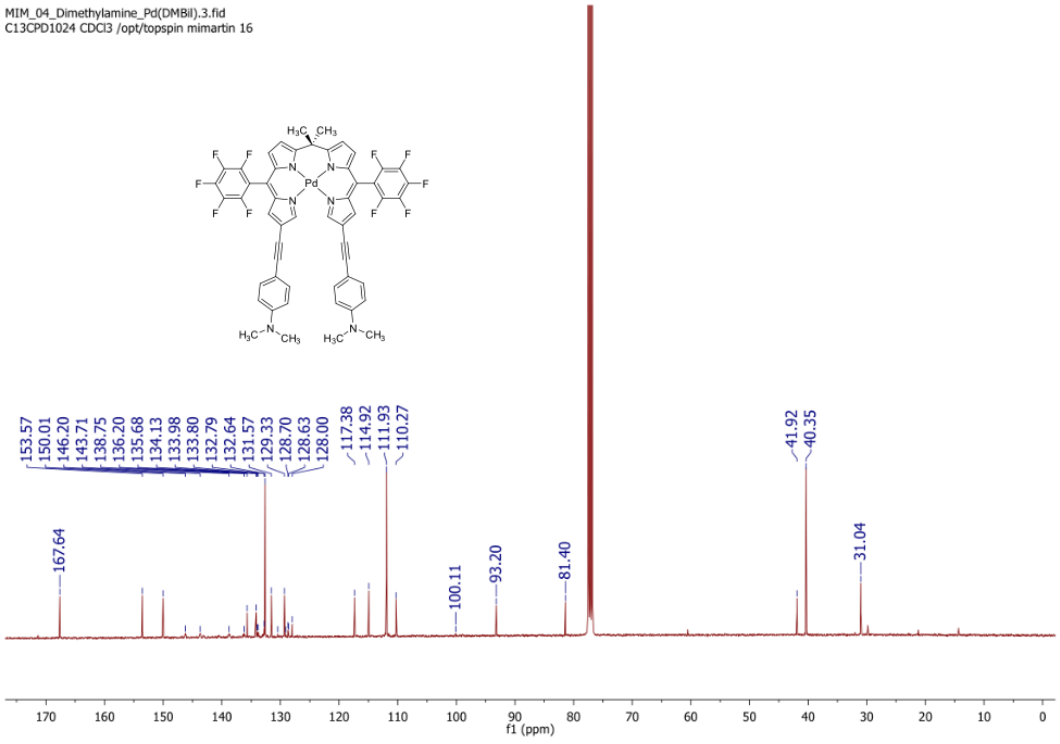

Figure S21. $^{13}C\{^1H\}$ NMR of **Pd[DMBil2–N(CH$_3$)$_2$]**

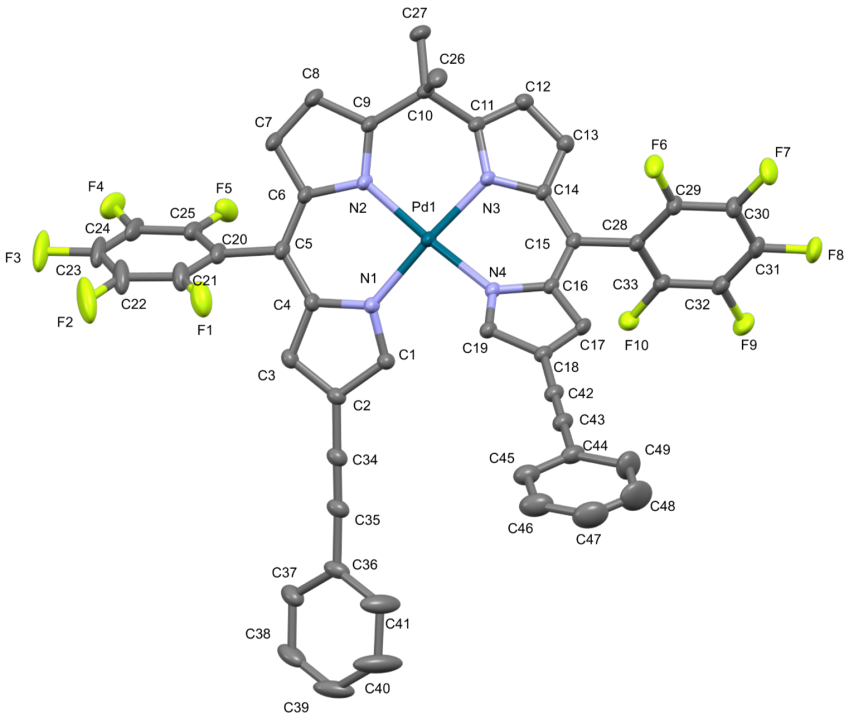

Figure S22. Fully labelled structure plot of **Pd[DMBil2–H]**. Atoms are shown as ellipsoids with 30% probability. Hydrogen atoms are omitted for clarity.

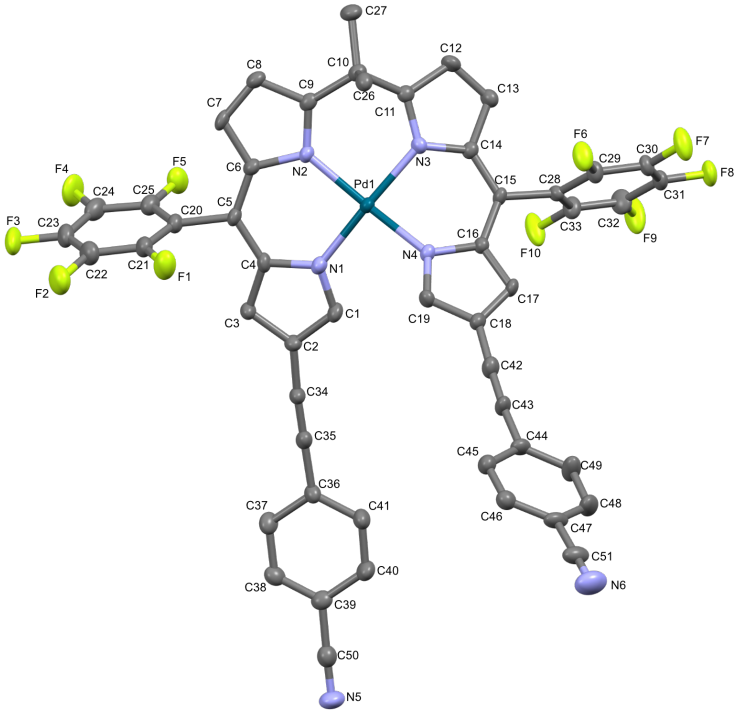

Figure S23. Fully labelled structure plot of **Pd[DMBil2–CN]**. Atoms are shown as ellipsoids with 30% probability. Two Pd[DMBil2–CN] residues (three residues in 1 unit cell) and hydrogen atoms are omitted for clarity.

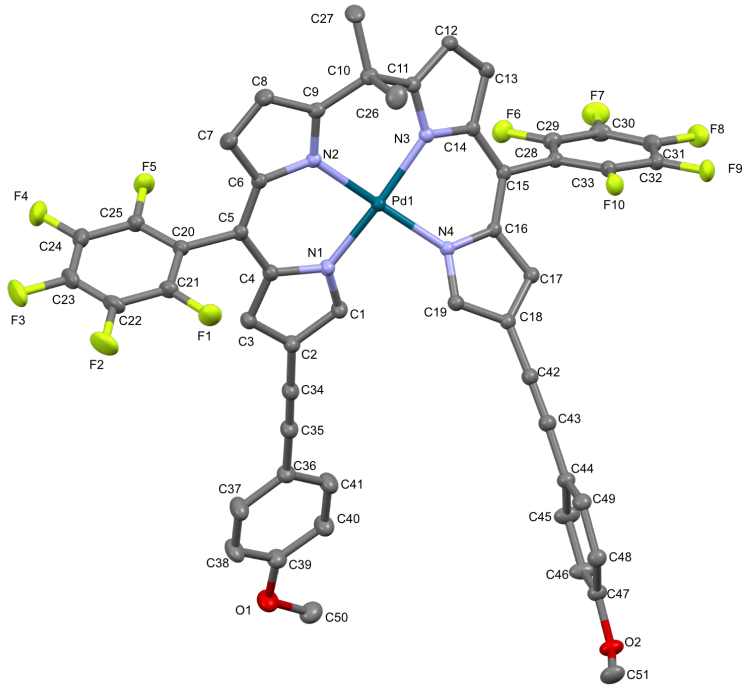

Figure S24. Fully labelled structure plot of **Pd[DMBil2–OCH$_3$]**. Atoms are shown as ellipsoids with 30% probability. Hydrogen atoms are omitted for clarity.

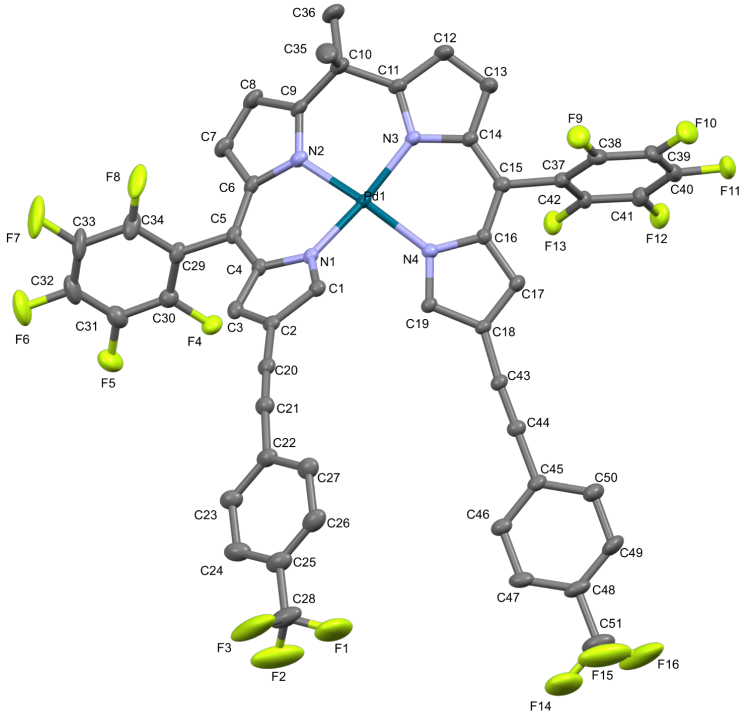

Figure S25. Fully labelled structure plot **of Pd[DMBil2–CF$_3$]**. Atoms are shown as ellipsoids with 30% probability. One Pd[DMBil2–CF$_3$] residue, two toluene molecules, and hydrogen atoms are omitted for clarity.

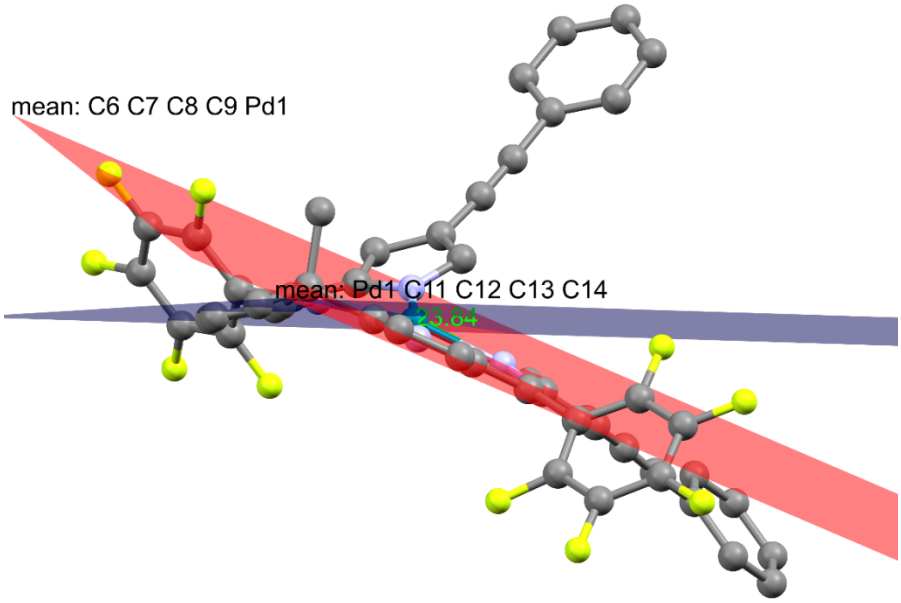

Figure S26. Illustration using **Pd[DMBil2–H]** to represent the planes used to determine internal pyrrole dihedral angles.

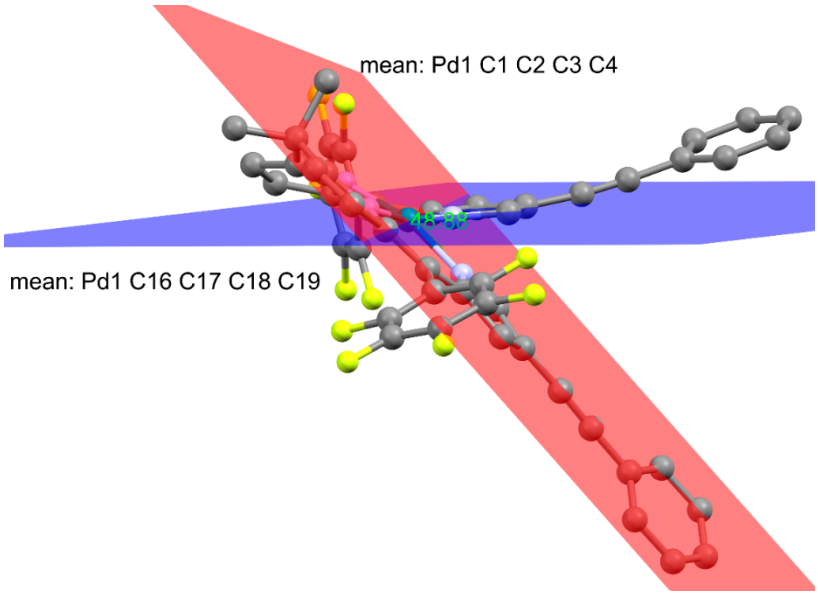

Figure S27. Illustration using **Pd[DMBil2–H]** to represent the planes used to determine external pyrrole dihedral angles.

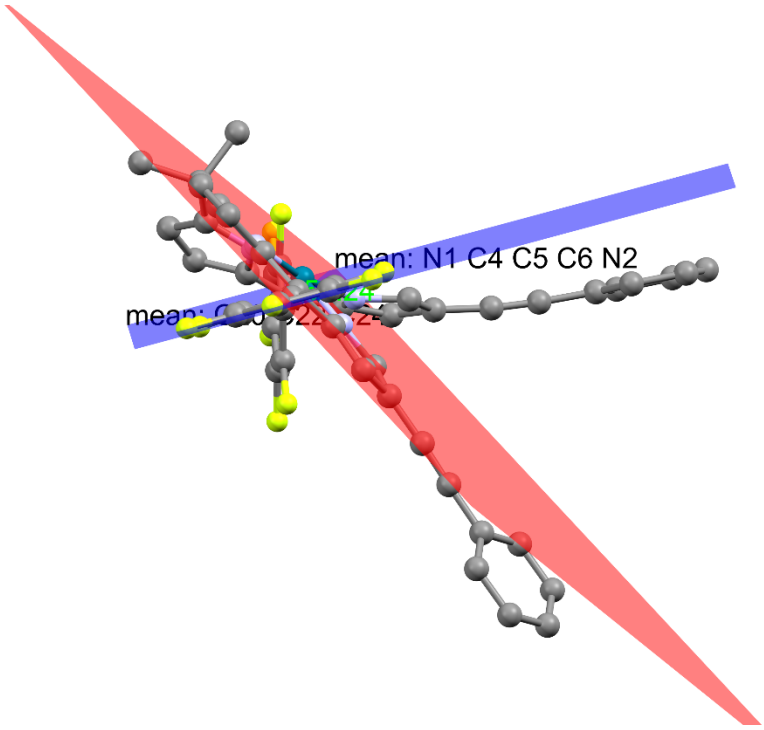

Figure S28. First illustration using **Pd[DMBil2–H]** to represent the planes used to determine C_6F_5-dipyrrole dihedral angles.

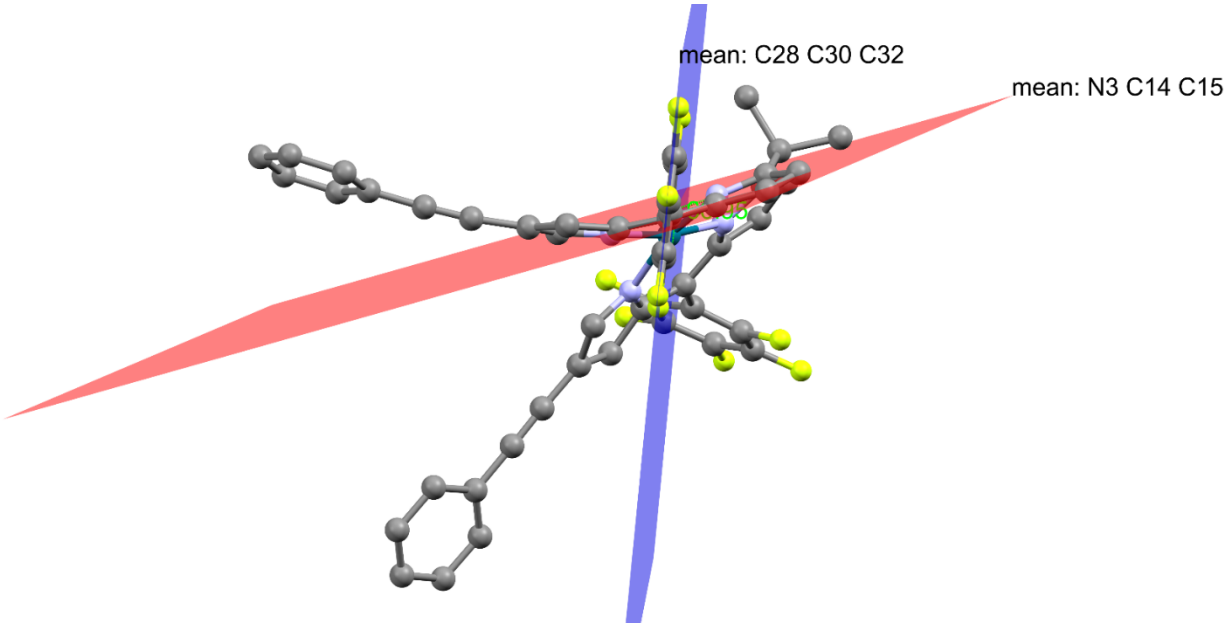

Figure S29. Second illustration using **Pd[DMBil2–H]** to represent the planes used to determine C_6F_5-dipyrrole dihedral angles

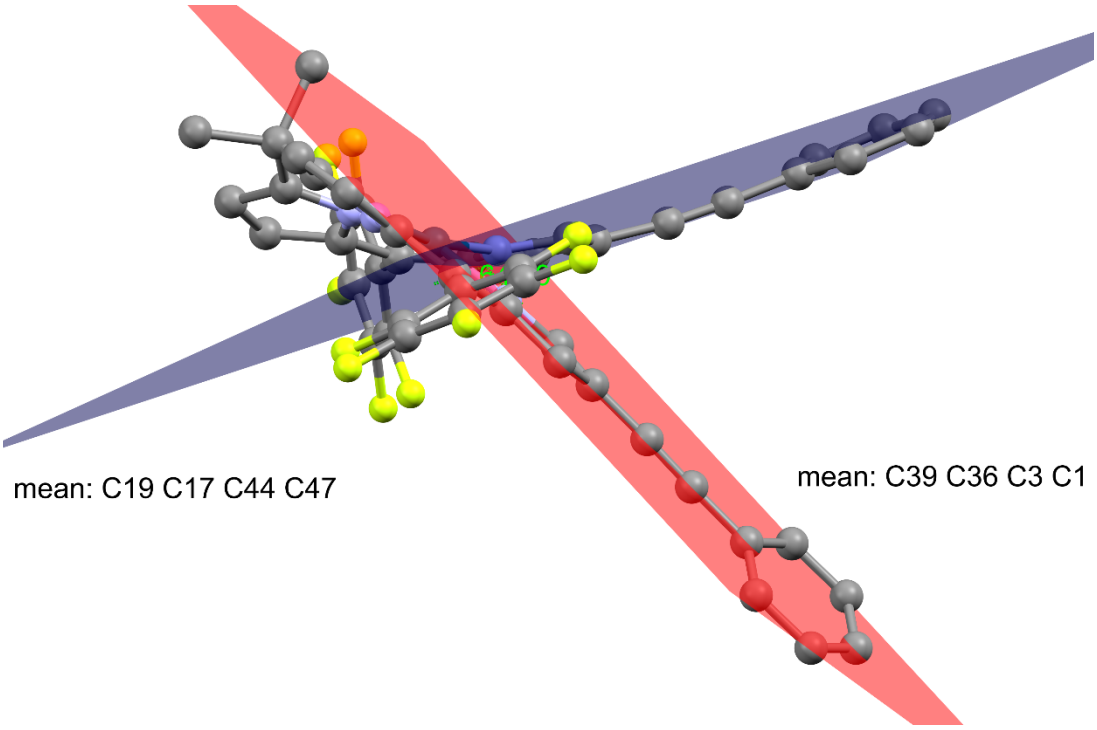

Figure S30. Illustration using **Pd[DMBiI2–H]** to represent the planes used to determine Ph-Pd-Ph dihedral angles.

Table S1: Crystallographic information for **Pd[DMBil2–CN]**, **Pd[DMBil2–CF_3]**, **Pd[DMBil2]**, and **Pd[DMBil2–OCH_3]**

	Pd[DMBil2–CN]	**Pd[DMBil2–CF_3]**	**Pd[DMBil2–H]**	**Pd[DMBil2–OCH_3]**
empirical formula	$C_{51}H_{22}F_{10}N_6Pd$	$C_{51}H_{22}F_{16}N4Pd$	$C_{49}H_{24}F_{10}N_4Pd$	$C_{51}H_{28}F_{10}N_4O_2Pd$
fw	1015.15	1226.04	965.12	1025.17
cryst syst	monoclinic	monoclinic	triclinic	monoclinic
space group	*Cc*	$P2_1/n$	*P*-1	*C2/c*
a	44.561(2) Å	20.7184(9) Å	13.1727(5) Å	32.1914(17) Å
b	11.8744(6) Å	15.4765(5) Å	13.2803(5) Å	9.8728(5) Å
c	31.6333(16) Å	34.4992(15) Å	15.2360(5) Å	30.9174(17) Å
α	90°	90°	90.573(1)°	90°
β	122.150(2)°	92.264(2)°	97.609(1)°	107.046(7)°
γ	90°	90°	109.207(1)°	90°
V	14171.5(13) $Å^3$	11000.1(8) $Å^3$	2490.73(16) $Å^3$	9394.5(9) $Å^3$
Z	12	8	2	8
temp	150(2) K	150(2) K	150(2) K	150(2) K
D_{calcd}	1.428 g/cm^3	1.481 g/cm^3	1.428 g/cm^3	1.450 g/cm^3
2Θ range	1.316°-27.640°	2.454°-76.059°	1.626°-37.387°	1.323°-30.636°
μ	0.474 mm^{-1} (Mo Kα)	3.588 mm^{-1} (Cu Kα)	0.444 mm^{-1} (Mo Kα)	0.479 mm^{-1} (Mo Kα)
Reflns	32731	21802	25629	14487
Unique	24931	18886	16629	12330
R(int)	0.0720	0.0733	0.0817	0.0442
R_1	0.0476	0.0638	0.0484	0.0357
wR_2	0.1140	0.1457	0.1497	0.0955

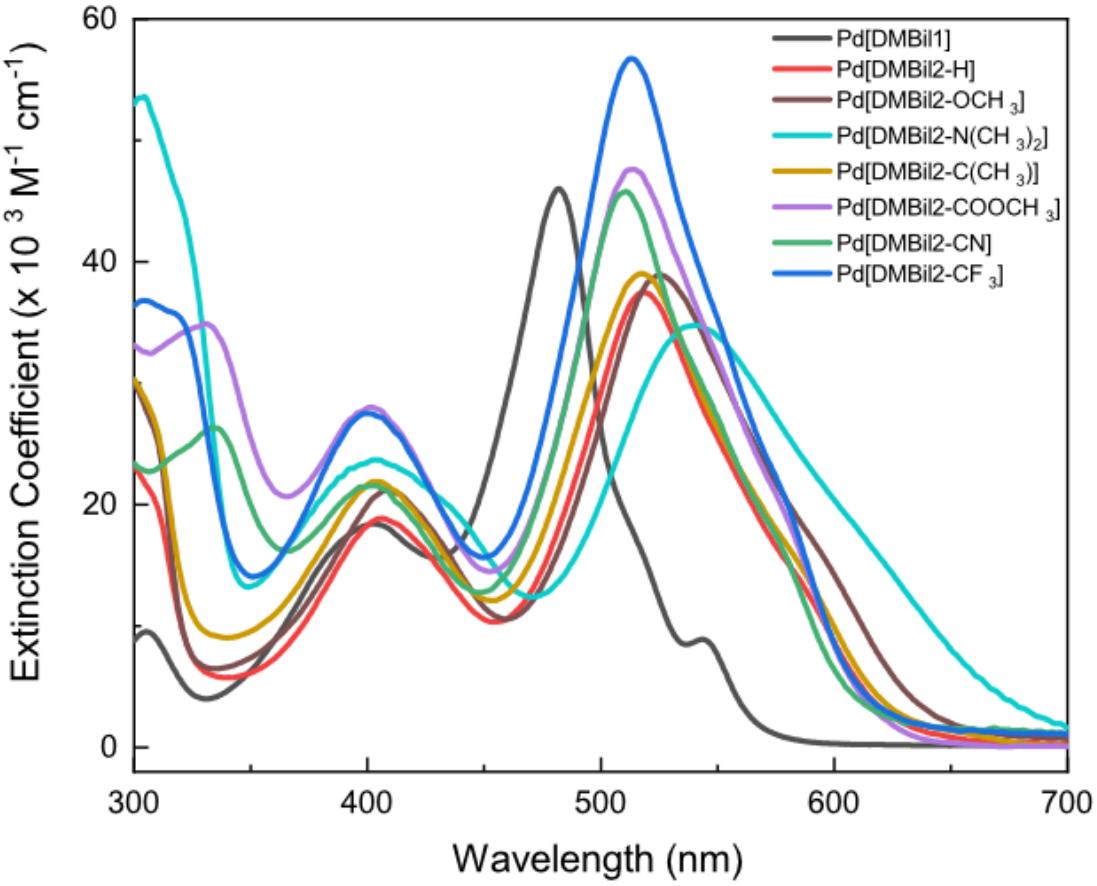

Figure S31: Absorption profiles for all **Pd[DMBil2–R]** derivatives in methanol.

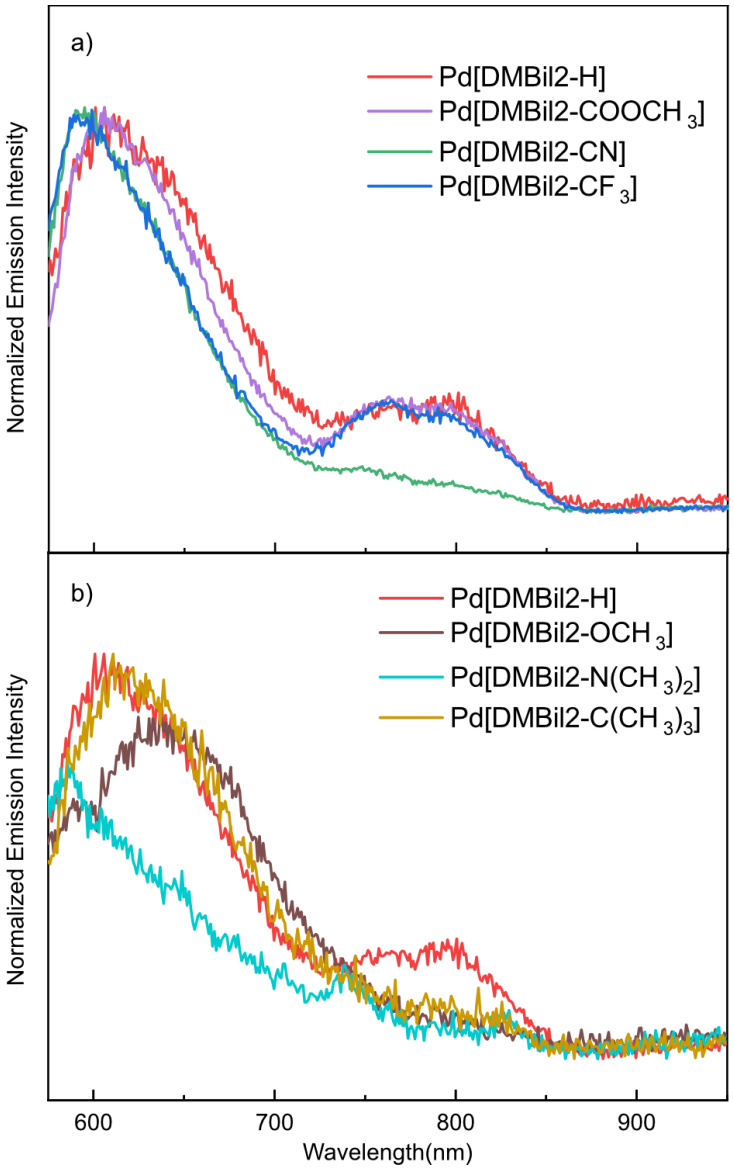

Figure S32: Emission profiles for all **Pd[DMBiI2–R]** derivatives in methanol.

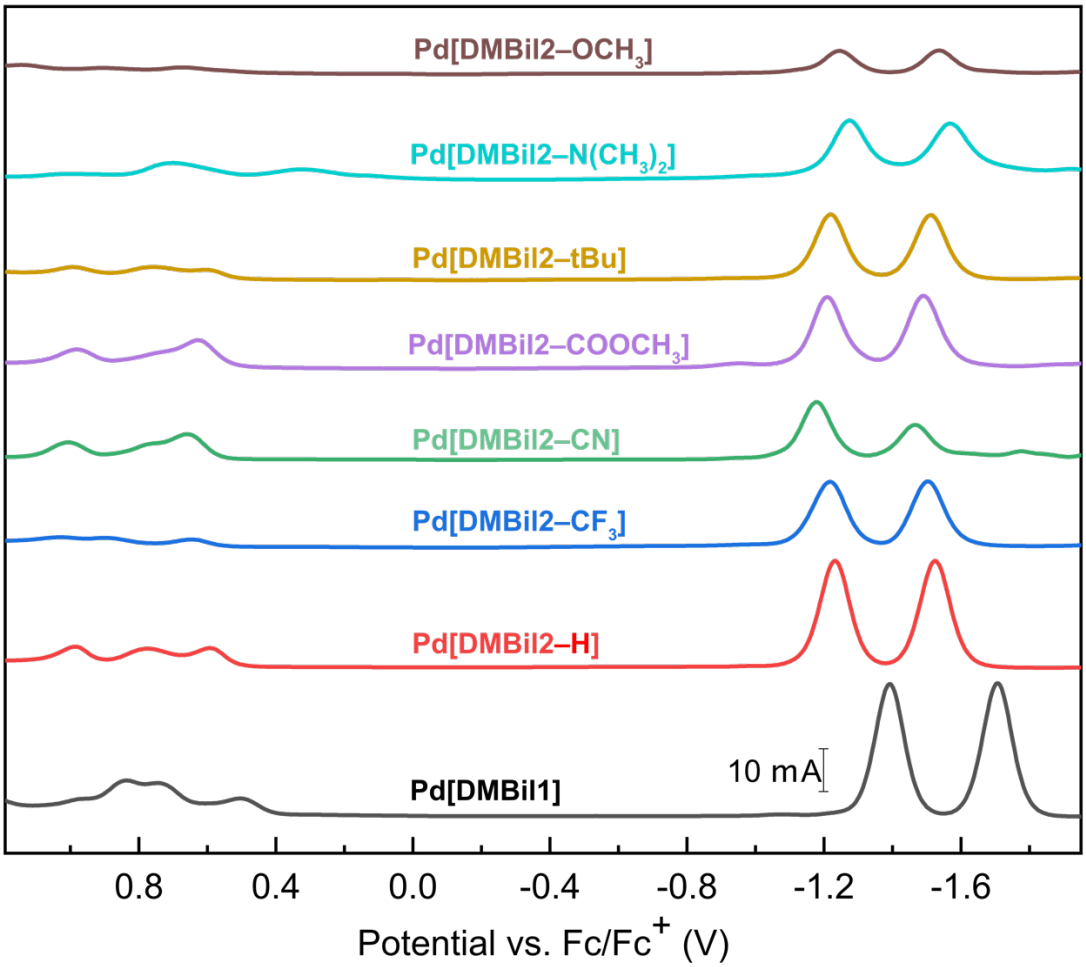

Figure S33. Stacked Differential Pulsed Voltammograms of **Pd[DMBil1]** and **Pd[DMBil2–R]** derivatives in anhydrous acetonitrile.

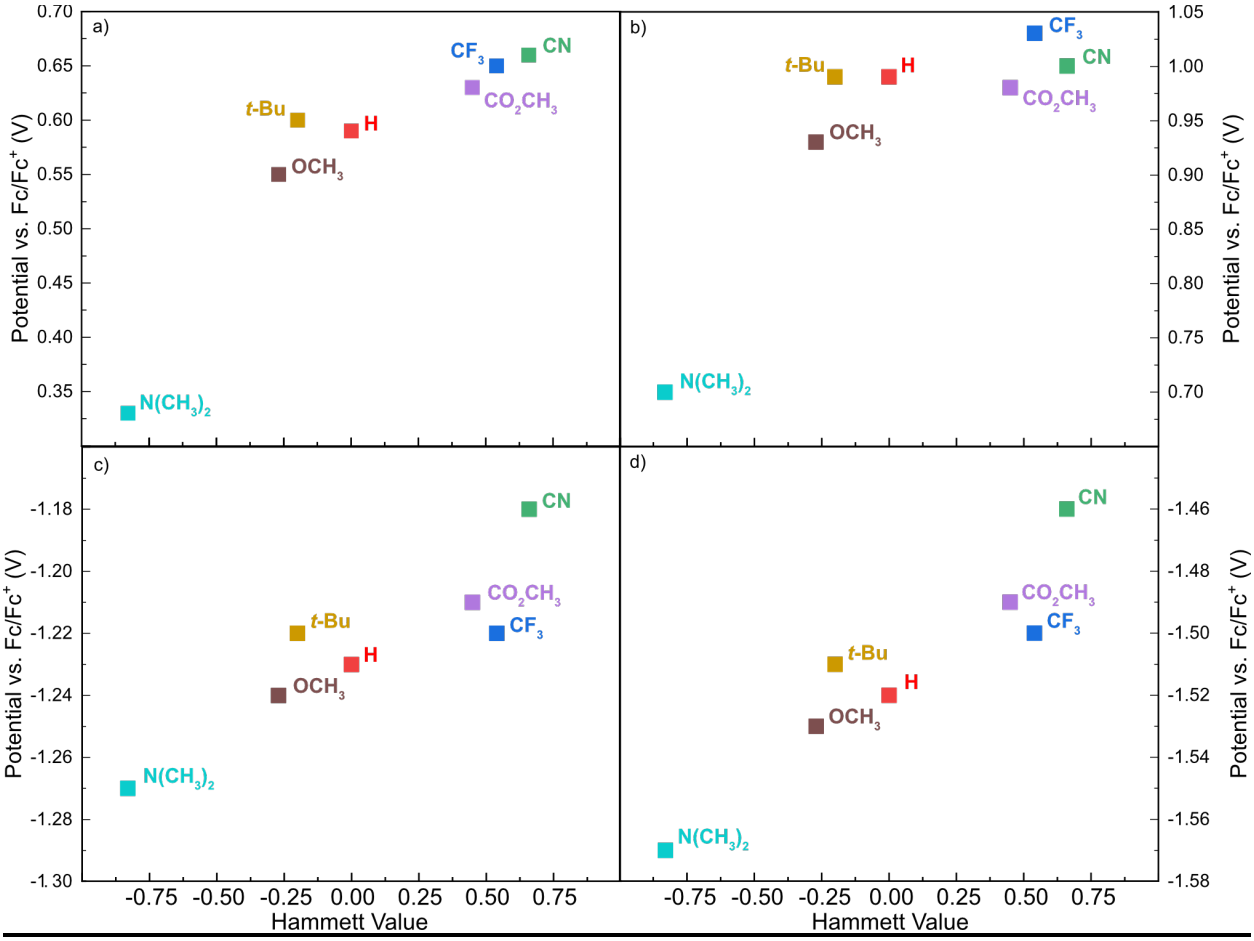

Figure S34: Scatter plots showing the relationship between *para*-Hammett values (σ_p) and a) the first oxidation potential, b) the second oxidation potential, c) the first reduction potential, and d) the second reduction potential.

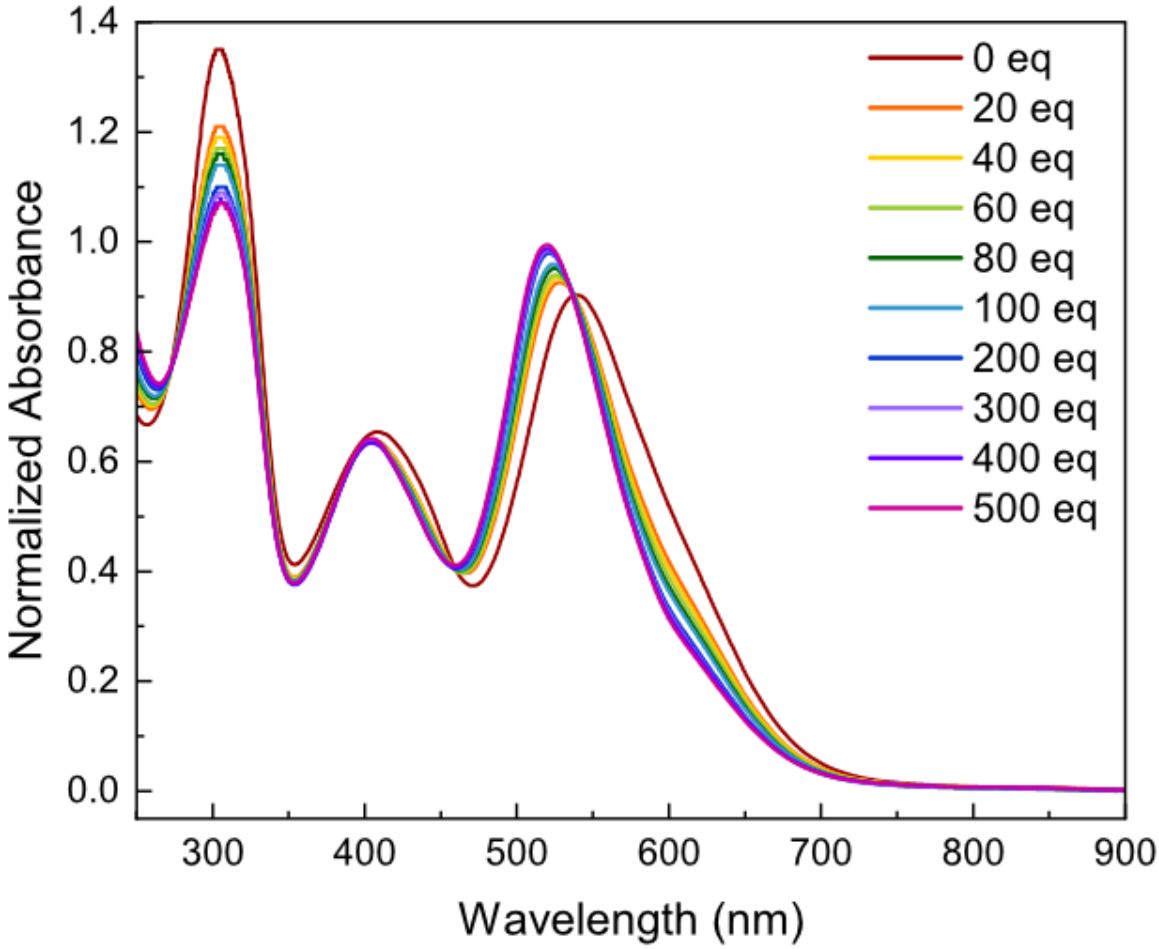

Figure S35: Absorption profiles recorded for **Pd[DMBiI2-N(CH_3)$_2$]** in methanol containing different equivalents of trifluoroacetic acid.

REFERENCES

(1) Pistner, A. J.; Pupillo, R. C.; Yap, G. P. A.; Lutterman, D. A.; Ma, Y.-Z.; Rosenthal, J. Electrochemical, Spectroscopic, and 1O2 Sensitization Characteristics of 10,10-Dimethylbiladiene Complexes of Zinc and Copper. *J. Phys. Chem. A* **2014**, *118* (45), 10639–10648. https://doi.org/10.1021/jp506412r.

(2) Pistner, A. J.; Yap, G. P. A.; Rosenthal, J. A Tetrapyrrole Macrocycle Displaying a Multielectron Redox Chemistry and Tunable Absorbance Profile. *J. Phys. Chem. C* **2012**, *116* (32), 16918–16924. https://doi.org/10.1021/jp3059382.

(3) O'Brien, A. Y.; McGann, J. P.; Geier, G. R. Dipyrromethane + Dipyrromethanedicarbinol Routes to an Electron Deficient Meso-Substituted Phlorin with Enhanced Stability. *J. Org. Chem.* **2007**, *72* (11), 4084–4092. https://doi.org/10.1021/jo070216k.

(4) Pistner, A. J.; Lutterman, D. A.; Ghidiu, M. J.; Ma, Y.-Z.; Rosenthal, J. Synthesis, Electrochemistry, and Photophysics of a Family of Phlorin Macrocycles That Display Cooperative Fluoride Binding. *J. Am. Chem. Soc.* **2013**, *135* (17), 6601–6607. https://doi.org/10.1021/ja401391z.

(5) Potocny, A. M.; Riley, R. S.; O'Sullivan, R. K.; Day, E. S.; Rosenthal, J. Photochemotherapeutic Properties of a Linear Tetrapyrrole Palladium(II) Complex Displaying an Exceptionally High Phototoxicity Index. *Inorg. Chem.* **2018**, *57* (17), 10608–10615. https://doi.org/10.1021/acs.inorgchem.8b01225.

(6) Rice, A. T.; Martin, M. I.; Warndorf, M. C.; Yap, G. P. A.; Rosenthal, J. Synthesis, Spectroscopic, and 1O2 Sensitization Characteristics of Extended Pd(II) 10,10-Dimethylbiladiene Complexes Bearing Alkynyl–Aryl Appendages. *Inorg. Chem.* **2021**, *60* (15), 11154–11163. https://doi.org/10.1021/acs.inorgchem.1c01127.

(7) Fulmer, G. R.; Miller, A. J. M.; Sherden, N. H.; Gottlieb, H. E.; Nudelman, A.; Stoltz, B. M.; Bercaw, J. E.; Goldberg, K. I. NMR Chemical Shifts of Trace Impurities: Common Laboratory Solvents, Organics, and Gases in Deuterated Solvents Relevant to the Organometallic Chemist. *Organometallics* **2010**, *29* (9), 2176–2179. https://doi.org/10.1021/om100106e.

(8) Filipovich, G.; Tiers, G. V. D. Fluorine N.s.r. Spectroscopy. I. Reliable Shielding Values, ø, by Use of CCl3F as Solvent and Internal Reference. *J. Phys. Chem.* **1959**, *63* (5), 761–763. https://doi.org/10.1021/j150575a040.

(9) *Apex3*; Bruker AXS Inc: Madison, WI, 2015.

(10) Sheldrick, G. M. SHELXT – Integrated Space-Group and Crystal-Structure Determination. *Acta Crystallogr. Sect. Found. Adv.* **2015**, *71* (1), 3–8. https://doi.org/10.1107/S2053273314026370.

(11) Sheldrick, G. M. Crystal Structure Refinement with SHELXL. *Acta Crystallogr. Sect. C Struct. Chem.* **2015**, *71* (1), 3–8. https://doi.org/10.1107/S2053229614024218.

(12) Spek, A. L. PLATON SQUEEZE: A Tool for the Calculation of the Disordered Solvent Contribution to the Calculated Structure Factors. *Acta Crystallogr. Sect. C Struct. Chem.* **2015**, *71* (1), 9–18. https://doi.org/10.1107/S2053229614024929.

(13) Brouwer, A. M. Standards for photoluminescence quantum yield measurements in solution (IUPAC Technical Report). *Pure Appl. Chem.* **2011**, *83* (12), 2213–2228. https://doi.org/10.1351/PAC-REP-10-09-31.

(14) Liu, Y.; Hammitt, R.; Lutterman, D. A.; Joyce, L. E.; Thummel, R. P.; Turro, C. Ru(II) Complexes of New Tridentate Ligands: Unexpected High Yield of Sensitized 1O2. *Inorg. Chem.* **2009**, *48* (1), 375–385. https://doi.org/10.1021/ic801636u.

(15) Hu, Q.-J.; Lu, Y.-C.; Yang, C.-X.; Yan, X.-P. Synthesis of Covalently Bonded Boron-Dipyrromethene–Diarylethene for Building a Stable Photosensitizer with Photo-Controlled Reversibility. *Chem. Commun.* **2016**, *52* (31), 5470–5473. https://doi.org/10.1039/C6CC01864E.